MODELING TEMPORAL PATTERNS OF NEURAL SYNCHRONIZATION: SYNAPTIC PLASTICITY AND STOCHASTIC MECHANISMS

A Dissertation

Submitted to the Faculty

of

Purdue University

by

Joel Zirkle

In Partial Fulfillment of the

Requirements for the Degree

of

Doctor of Philosophy

August 2020

Purdue University

Indianapolis, Indiana

THE PURDUE UNIVERSITY GRADUATE SCHOOL
STATEMENT OF DISSERTATION APPROVAL

Dr. Leonid Rubchinsky, Chair

Department of Mathematical Sciences

Dr. Alexey Kuznetsov

Department of Mathematical Sciences

Dr. Jared Barber

Department of Mathematical Sciences

Dr. Julia Arciero

Department of Mathematical Sciences

Approved by:

Dr. Evgeny Mukhin

Head of the Graduate Program

To Champ, a real scientist

ACKNOWLEDGMENTS

I'd like to thank my advisor, Dr. Leonid Rubchinsky, for his guidance and genuinely warm nature. His diverse knowledge led to many interesting conversations and I appreciate his direction over the past four years. I certainly still have much to learn, but he has gotten me started on an exciting track forward.

To all the IUPUI friends over the years, thank you for the memories. Thank you to Josiah Baker for basically convincing me to study math in the first place. Thank you to Dr. Kevin Berkopes for creating the MAC ennvironment that has to be the highlight of my undergraduate years. Not only did we have lots of laughs, but I wouldn't have started graduate school as strong mathematically had it not been for the years of practice at the MAC. To Jens, the Saunders, Ahmad, Anthony and Thomas Yahl for many unforgettable times. To Champ for his patience during some long days, and for always giving me a reason to smile. And of course to my family, who are a great support should you need them. And oddly, to Burnsville, NC where I find myself at the end. You provided the ideal environment to finish everything I needed to do.

TABLE OF CONTENTS

Page

LIST OF TABLES

LIST OF FIGURES

Figure Page

Figure Page

Figure Page

Figure Page

ABSTRACT

Zirkle, Joel Ph.D., Purdue University, August 2020. Modeling Temporal Patterns of Neural Synchronization: Synaptic Plasticity and Stochastic Mechanisms. Major Professor: Leonid Rubchinsky.

Neural synchrony in the brain at rest is usually variable and intermittent, thus intervals of predominantly synchronized activity are interrupted by intervals of desynchronized activity. Prior studies suggested that this temporal structure of the weakly synchronous activity might be functionally significant: many short desynchronizations may be functionally different from few long desynchronizations, even if the average synchrony level is the same. In this thesis, we use computational neuroscience methods to investigate the effects of (i) spike-timing dependent plasticity (STDP) and (ii) noise on the temporal patterns of synchronization in a simple model. The model is composed of two conductance-based neurons connected via excitatory unidirectional synapses. In (i) these excitatory synapses are made plastic, in (ii) two different types of noise implementation to model the stochasticity of membrane ion channels is considered. The plasticity results are taken from our recently published article [47], while the noise results are currently being compiled into a manuscript.

The dynamics of this network is subjected to the time-series analysis methods used in prior experimental studies. We provide numerical evidence that both STDP and channel noise can alter the synchronized dynamics in the network in several ways. This depends on the time scale that plasticity acts on and the intensity of the noise. However, in general, the action of STDP and noise in the simple network considered here is to promote dynamics with short desynchronizations (i.e. dynamics reminiscent of that observed in experimental studies) over dynamics with longer desynchronizations.

1. INTRODUCTION

This thesis concerns itself with the inherent temporal patterns of synchronization within neural systems. This is a numerical modeling study, where we adapt a conductance-based model to our neural network to study the resulting synchrony in a simple and general setting. Since our model is highly nonlinear and the parameters we are interested in are not small, it is natural to use numerical methods. To understand the construction of the mathematical model that will be used throughout this thesis, it is necessary to understand some basic neuronal electrophysiology. This is very briefly summarized in section 1.1 and is largely based on [1–3]. In section 1.3, a brief introduction to synchronization of oscillators is given. Lastly, in section 1.4 the problem that is studied in this thesis is stated and previous studies conducted on experimental data are mentioned as motivation.

1.1 Basic Neuronal Electrophysiology and its Mathematical Modeling

In this thesis we only consider single-compartment models. This means that we neglect all spatial components and model the neuronal membrane voltage using a system of ordinary differential equations. Naturally, a real biological neuron is composed of different sections (e.g. soma, axon, dendrite tree), and the overall geometry of a neuron may be quite complicated. While this geometry can affect some properties of the neuron [2], we wish to study synchronicity in a more general setting.

The membrane of a neuron is composed of a lipid bilayer that acts as a physical barrier to the movement of ionic species. Generally speaking, in a neuron at rest there is an excess of negatively charged ions within the neuron, and a net positive charge

in the extracellular medium. Due to this setup, the neuronal membrane effectively acts as a capacitor and we may model it using (1.1).

$$C\frac{\mathrm{d}v}{\mathrm{d}t} = \frac{\mathrm{d}Q}{\mathrm{d}t} \tag{1.1}$$

Here C is the membrane capacitance, v is the potential difference across the membrane (aka the neural voltage) and the time-derivative of Q represents current moving across the membrane.

Transmembrane current is generated by the movement of ions through ion channels: large proteins that bridge the neural membrane and allow ions to move into, and out of, the cell. There is a large number of currents at play, however, we will restrict ourselves to three: a leak current, a delayed-rectified potassium current and a persistent sodium current. We use Ohm's Law to describe the amount of current that flows through these ion channels, (1.2).

$$I = g(V - E) \tag{1.2}$$

Where I is the current, $g = 1/r$ is the reciprocal of resistance and is called the conductance of the ion channel, and $V - E$ is a potential difference that acts as a driving force for the current. E is the reversal potential for the specific ionic species and is often calculated using the Nernst equation. Physically it describes the potential at which the current would reverse the direction of its flow. Ion channels are often selective for a single ionic species, e.g. a sodium ion channels will only allow sodium ions to move through them. This means that we need a separate term for each type of current we use. In our case we have the three currents listed in (1.3).

$$I_{Na} = g_{Na}(V - E_{Na}), \qquad I_K = g_K(V - E_K), \qquad I_L = g_L(V - E_L) \tag{1.3}$$

The first two currents are the sodium and potassium currents, respectively. In the last term, the subscript L refers to the so-called "leakage current". This current accounts for all the time-independent processes that affect the neural voltage, e.g. ion pumps

that exchange certain ratios of ions across the neural membrane and are responsible for maintaining the resting potential of the neuron.

At this point we summarize our discussion by drawing what is often called the "equivalent circuit". That is, we are modeling a neuron as a circuit where the membrane is a capacitor, the ion channels are resistors and each ionic species provides an electromotive force. The equivalent circuit for the mathematical model that we will be using, the Morris-Lecar (ML) model, is given in Figure 1.1.

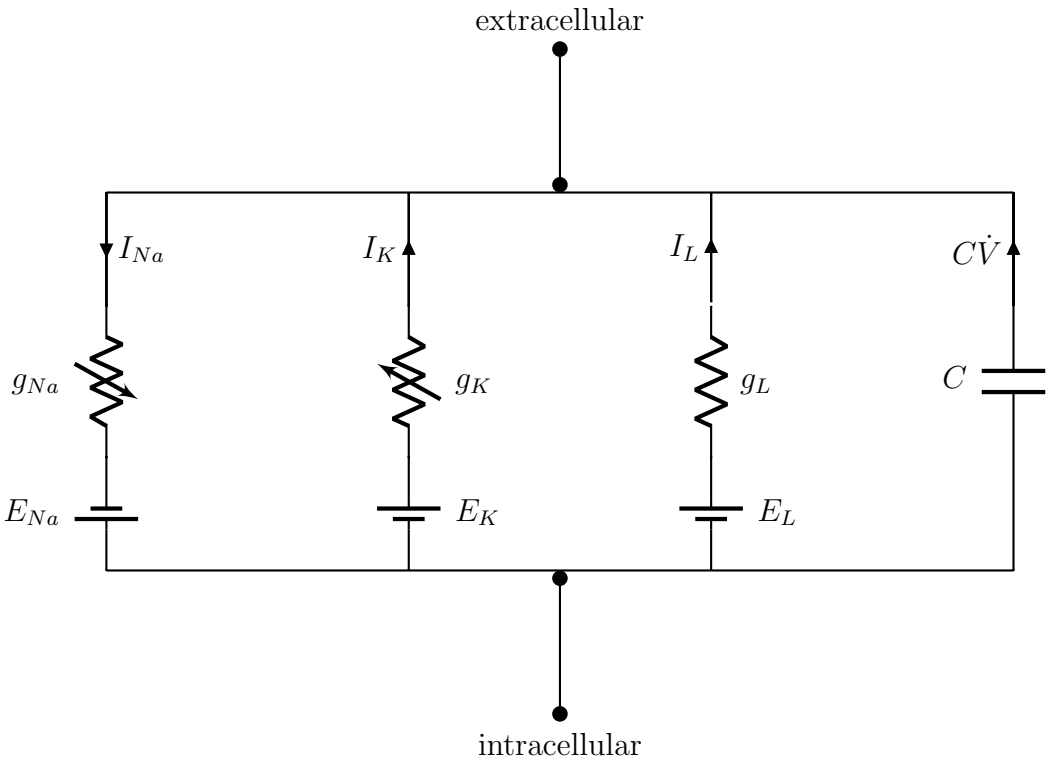

Figure 1.1. Equivalent circuit for a Morris-Lecar neuron. Adapted from [1]

Before we write down the differential equations that will govern the neural voltage, there is one additional feature of ion channels that we need to address. In Figure 1.1 it is seen that the conductances for the sodium and potassium chan-

nels are time-varying. This is because these types of channels are voltage-gated: the channel conductance depends on the neural voltage. Furthermore, ion channels have two mechanisms by which they either activate/deactivate (open/close) or inactivate/deinactivate (close/open). The conductance of an ion channel can then be modeled as:

$$g_i = \overline{g}_i m^a h^b. \tag{1.4}$$

The quantity $\overline{g}$ represents the maximal conductance of that ion channel (the conductance if every ion channel of that type was open), m is the probability that the mechanism that activates is open and h is the probability that the mechanism that inactivates is open. a and b are positive integers that represent the number of each mechanism of each type in a single ion channel. The variables m and h are dynamic quantities that are modeled according to the first-order kinetic equation (1.5).

$$\frac{\mathrm{d}X}{\mathrm{d}t} = \alpha_X(v)(1 - X) - \beta_X(v)X \tag{1.5}$$

X is a generic variable representing either an activating or inactivating probability. The coefficients $\alpha_X(v)$ and $\beta_X(v)$ are voltage-dependent opening and closing rates, respectively, for the ion channel. We can rewrite (1.5) as:

$$\tau_X(v)\,\frac{\mathrm{d}X}{\mathrm{d}t} = X_\infty(v) - X. \tag{1.6}$$

(1.6) says that the quantity X approaches it's steady-state value, X_∞, on the time-scale τ_X. Using an argument based on thermodynamics [3], we expect both α_X and β_X to be proportional to a decaying exponential function, i.e. $\alpha_X, \beta_X \propto \exp(-f(v))$. Hence the steady-state function X_∞ is sigmoidal, and the time-constant τ_X is unimodal.

In the ML model we have two voltage-dependent conductances. The sodium conductance is given in (1.7), the potassium conductance in (1.8). To arrive at (1.7) we make the assumption that the sodium current activates instantaneously relative to the activation of the potassium current. Comparison of the time-constants τ_{Na}

and τ_K shows that this is generally a good approximation. The benefit of replacing the dynamic variable m with its steady-state value m_∞ reduces the dimension needed for the system of differential equations. The variable w represents the proportion of potassium channels that are open; it is governed by an equation of the form of (1.6).

$$g_{Na} = \overline{g}_{Na} m_\infty(v) \tag{1.7}$$

$$g_K = \overline{g}_K w \tag{1.8}$$

We are now ready to write down the system of differential equations that is the ML model, see (1.9) and (1.10). In chapter 2 we expand on the mathematical description of the ML model, so for now it is enough to understand where each term in the model is derived from. From the equivalent circuit (see Figure 1.1) and Kirchoff's Law we obtain the voltage equation (1.9), the variable v represents the neuronal membrane voltage. The activation variable for potassium is controlled by equation (1.10).

$$\frac{\mathrm{d}v}{\mathrm{d}t} = -\bar{g}_{Na} m_\infty(v)(v - v_{Na}) - \bar{g}_K w(v - v_K) - \bar{g}_L(v - v_L) + I \tag{1.9}$$

$$\frac{\mathrm{d}w}{\mathrm{d}t} = \frac{w_\infty(v) - w}{\tau(v)} \tag{1.10}$$

The term I in (1.9) represents any external current to the neuron. It is this external action that perturbs a neuron's membrane potential and allows it to deviate from its resting value.

1.2 The Action Potential

Using our basic understanding of neural electrophysiology, we now give a detailed description of the generation of an action potential. Briefly, an action potential is a sharp and dramatic increase (depolarization) of the membrane potential followed by a sharp decrease (hyperpolarization) that brings the membrane potential back to rest.

In Figure 1.2 we simulate a ML neuron and inject a current pulse (plot D). This externally applied current is sufficiently strong to evoke an action potential, as seen in

plot A. We split the action potential into two parts: the upstroke and the downstroke. Before we begin, we mention that we have the following ordering of reversal potentials: $E_K < E_{rest} < E_{Na}$, where E_{rest} is the resting potential of the neuron. The reversal potential helps determine the driving force of a current, which leads to two important consequences. The first is that sodium current tends to depolarize a neuron's membrane, while the potassium current wants to hyperpolarize the membrane. In other words, as we shall see, the sodium current will be responsible for the upstroke of an action potential while the potassium current will be responsible for the downstroke. The second consequence is the sign convention for currents. If $v < E$ the current corresponding to E will be negative, and if $v > E$ the current is positive. Physiologically, if $E_K < v < E_{Na}$ then Na^+ ions tend to flow into the cell while K^+ ions tends to flow out of the cell. Since we classify current as the flow of positive charges, we use the convention that a current is positive if it flows out of the cell. The exception here is that we say a current that is injected from outside directly into the neuron is positive.

In Figure 1.2 the externally applied current is positive which causes a depolarization of the neuron's membrane. As the membrane depolarizes, the voltage-gated sodium channels begin to open, as demonstrated in the conductances plot (plot B). This allows Na^+ ions to flow into the cell, causing further depolarization. This positive feedback loop is what causes the rapid depolarization during the upstroke of an action potential.

As the neuron's voltage approaches the reversal potential for sodium, the driving force for the sodium current approaches zero. During this time, the slower potassium channels have opened, allowing K^+ ions to flow out of the cell. For a short period of time, the opposite effects of the sodium and potassium currents somewhat cancel each other, making the hyperpolarization slow.

As the potassium current continues to activate and hyperpolarize the membrane, the sodium current (which is very fast comparatively) deactivates. This leaves behind the potassium current, which rapidly hyperpolarizes the cell. In fact, because $E_K < E_{rest}$ and because the potassium current is slow to deactivate, the membrane potential is pushed below its resting potential and the neuron experiences a refractory period.

Lastly, given enough time, the potassium current deactivates and the potential of the membrane is brought back to its resting value via the leak current (physiologically through ion pumps). A constant current applied for a long enough time, or some other varying form of current impulse, could induce multiple spikes.

1.3 Synchrony

The notion of synchronization is well-documented in the natural and physical sciences. In particular, the evidence of synchronization in biological systems ranges from some species of fireflies that flash in synchrony in certain areas in southeast Asia [24] to human circadian rhythms to the interaction of glucose and insulin in the human body [4] to the different gaits that animals use for movement [25]. Within the context of neuroscience, synchrony is pervasive and plays a role in sensory systems (visual, auditory, olfactory), some cognitive functions such as holding attention, motor control such as breathing or walking, generation of electroencephalography (EEG) and magnetoencephalography (MEG) signals, and memory [26–33]. In the public health domain there are several well-known neurological disorders - such as epilepsy, Alzheimer's disease, Parkinson's disease, and schizophrenia - that are associated with abnormal synchrony (either too weak or too strong) [4, 34–38].

The phenomenon of synchronization described in this thesis is that between two weakly coupled self-sustained limit cycle oscillators (neurons). They are self-sustained

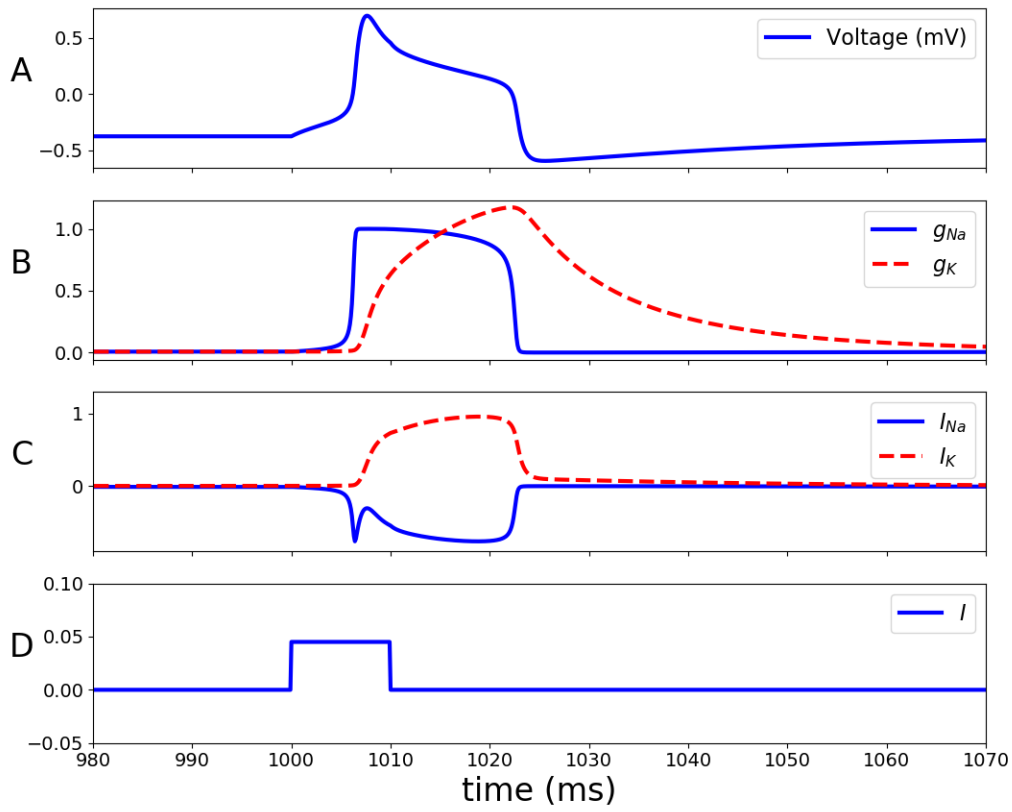

Figure 1.2. Demonstration of an action potential in a ML neuron. On each subplot the horizontal axis represents time and the vertical axes from top to bottom are voltage, conductances, membrane currents and externally applied current pulse. We note that the model is scaled such that voltage is mV, time is ms, the conductances are mS/mm^2 and the current is mA. However, it is conventional here to not use units for the conductances. Adapted from [1].

in the sense that they have an energy source (an externally applied current) that counteracts the natural energy dissipation that occurs in non-conservative systems. Since these are non-conservative systems, the oscillations are described by limit cycles. And the coupling takes the form of two unidirectional chemical synapses that connect the two neurons to each other. This coupling is made weak by setting the synaptic con-

ductance (analogous to an ion channel conductance) to a value significantly smaller than the conductances that control the inherent currents of each neuron.

For the definition of synchrony we take the phase-locking approach. First this requires that we define what phase is. There are several definitions that one may use to reconstruct the phase of an oscillator, the most common of which are the Hilbert transform, a geometric definition based on the inverse tangent, or a periodic piecewise linear function defined between certain events. However one wishes to define the phase function, it describes the same occurrence in the state space: the phase function tracks a state point on the limit cycle of the oscillator as the point makes one full cycle. Note that all phase functions are periodic, usually with a period of 2π or 1.

If $\phi_1(t)$ describes the phase of one neuron and $\phi_2(t)$ describes the phase of the second neuron, then phase-locking between the neurons is described as:

$$p\phi_1 - q\phi_2 < \text{constant} \tag{1.11}$$

where p, q are integers. The choice of the constant on the right-hand side of the inequality above is chosen based upon the specific problem being studied (see chapter 3). Often, (1.11) holds only for certain intervals of time [4, 39], which leads to the notion of transient synchrony: a system may exhibit synchronous behavior according to (1.11), interspersed with periods of desynchronous behavior. If we plot the unwrapped (not periodic) phase difference between two oscillators as a function of time, then transient synchrony presents itself as horizontal epochs separated by phase-slips, see Figure 1.3.

Another way to detect synchrony in a system is with what is commonly known as a first-return map (aka a Poincaré map). In chapter 3, where we detail the exact numerical methods used to quantify synchrony, we refer to this as a stroboscopic map. We opt to use this terminology as it evokes an intuitive sense of how the map

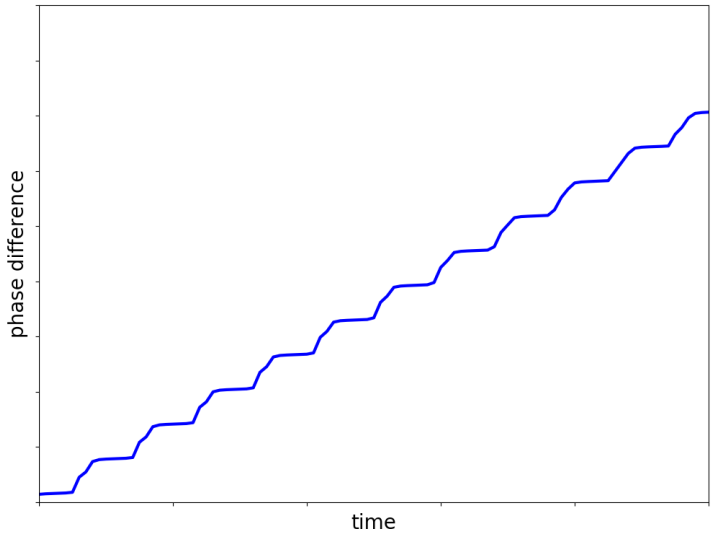

Figure 1.3. The unwrapped phase difference between two oscillators plotted as a function of time.

is created. A rigorous mathematical definition is given in [45, 46], along with simple examples where the first-return map can be expressed analytically. We find the stroboscopic map numerically, so here we only provide a quick sketch of the mathematical ideas.

We are given some periodic orbit of an n-dimensional dynamical system. In our case, we look at the periodic phase of our planar system. At an arbitrarily chosen location on the periodic orbit, we intersect the orbit with a hypersurface of dimension $n-1$. This hypersurface should be oriented such that the flow of the orbit is transverse to it. Then as the dynamical system evolves, the sequence of points of intersection between the hypersurface and the periodic orbit comprise the first-return map.

When we have two dynamical systems coupled together (as we do in this thesis), we slightly modify the above description. Now we have two periodic oscillatory quantities; the phase of each dynamical system. We again intersect the periodic orbit of the phase of one system at an arbitrary location with a hypersurface. At the time when the periodic orbit intersects this hypersurface, we record the value of the phase of the second dynamical system. This sequence of phase values is what we call the stroboscopic map. The idea behind the word "stroboscopic" is that we only view the phases of the two systems during brief flashes of time, in the same way that a dark room is illuminated by a strobe light only for brief flashes of time. Since the phase of the first system is relatively fixed, synchronization between the oscillators presents itself as fixed points of the stroboscopic map.

1.4 Motivation

Recent developments in time-series analysis allowed for the exploration of the temporal patterning of synchronized activity in brain dynamics on very short time-scales. Studies of different brain signals in different conditions and species suggest an apparently universal feature: synchronous activity is interrupted by very short (although potentially numerous) intervals of desynchronized dynamics (as opposed to few longer desynchronized episodes). This phenomenon was observed in the synchrony between local field potentials (LFPs) and spikes in different parts of the basal ganglia and EEG in Parkinson's disease [40–42], in synchronization between LFPs recorded in the prefrontal cortex and hippocampus of normal and amphetamine-sensitized mice [43], in the EEG of healthy human subjects [14], and in EEGs in autism spectrum disorders [44]. The differences in the temporal patterning are correlated with certain behavioral features, but the prevalence of short desynchronizations persisted nevertheless [42–44]. Therefore, short desynchronizations may be functionally important and the properties and mechanisms of desynchronization durations merit study.

These observations of the persistence of short desynchronizations naturally suggests the question about the biological mechanism(s) behind this phenomenon. The modeling study [11] suggested one possible mechanism: the short desynchronization dynamics was promoted by the substantial difference in the time-scales of spike-producing sodium and potassium currents. The relative slowness of the potassium delayed-rectifier current may be one of the reasons for why short desynchronizations are observed in different neural systems. However, there may also be other mechanisms. This thesis is aimed at the exploration of two potential mechanisms: one related to synaptic plasticity, and the other to the inherent stochasticity of real neural systems.

Chapters 2 and 3 provide the necessary details about the mathematical model and the method of sychronization analysis. Chapter 4 briefly summarizes the previous results of the modeling study [11], and explains the effects of certain parameters on the model. The intent of chapter 4 is to provide the reader with some intuition for the subsequent chapters. In chapter 5 we use computational modeling to explore how spike-timing dependent plasticity (STDP) can affect the temporal patterning of neural synchrony on short timescales. Then in chapter 6 we explore the effect of one source of noise in neural systems on the temporal patterns of synchrony.

2. MATHEMATICAL MODEL

2.1 Neuronal Model

Throughout the entirety of this thesis we will model each neuron using a two-dimensional conductance-based system of ordinary differential equations (ODEs). Izhikevich in [1] refers to this model as the "persistent sodium plus potassium model", and while this is very descriptive, it is mathematically equivalent to the more well-known Morris-Lecar (ML) model and will be referred to as such henceforth [1,2]. The model is given in equations (2.1) and (2.2) and is described below.

$$\frac{\mathrm{d}v_i}{\mathrm{d}t} = -I_{Na} - I_K - I_L - I_{syn} + I_{app} \tag{2.1}$$

$$\frac{\mathrm{d}w_i}{\mathrm{d}t} = \frac{w_\infty(v_i) - w_i}{\tau(v_i)} \tag{2.2}$$

The variable v_i in equation (2.1) describes the time-evolution of the i-th neuron's voltage. The first three terms are the sodium current, delayed rectifier potassium current and leak current, respectively. The expressions for these currents are given below in equations (2.3)–(2.5).

$$I_{Na} = \bar{g}_{Na} m_\infty(v_i)(v_i - v_{Na}) \tag{2.3}$$

$$I_K = \bar{g}_K w_i (v_i - v_K) \tag{2.4}$$

$$I_L = \bar{g}_L (v_i - v_L) \tag{2.5}$$

The sodium current is assumed to activate instantaneously and also to have no inactivation (hence the naming "persistent sodium..." in [1]). We can see this in equation (2.3) where in place of a dynamical variable m, that would describe the activation of the sodium current, instead we see the steady-state function $m_\infty(v_i)$. The activation of potassium current is much slower and is controlled by the variable w in (2.2), which represents the proportion of potassium ion channels that are open.

The leak current is an Ohmic current, i.e. the conductance g_L is constant.

The variables $\bar{g}_{Na}$, $\bar{g}_K$ and $\bar{g}_L$ are the maximal conductances for the sodium, potassium and leak currents, respectively. The steady-state functions for the gating variables of the sodium and potassium currents are given in equations (2.6) and (2.7).

$$m_\infty(v_i) = \frac{1}{1 + \exp\left(-2\dfrac{v_i - v_{m1}}{v_{m2}}\right)} \tag{2.6}$$

$$w_\infty(v_i) = \frac{1}{1 + \exp\left(-2\dfrac{v_i - v_{w1}}{\beta}\right)} \tag{2.7}$$

The voltage-dependent activation time constant of the potassium current is given in (2.8).

$$\tau(v_i) = \frac{2}{\epsilon_i\left(\exp\left(\dfrac{v_i - v_{w1}}{2\beta}\right) + \exp\left(\dfrac{v_{w1} - v_i}{2\beta}\right)\right)} \tag{2.8}$$

The functions in equations (2.6)–(2.8) are plotted in Figure 2.1. Figure 2.1(a) shows the steady-state functions m_∞ and w_∞. There are two features to point out here. First, the functions are sigmoidal; this means that at low voltages the currents are inactivated and only activate once the neuron starts becoming depolarized. The second feature is that the potassium steady-state function (the red dashed curve) is delayed (i.e. shifted to higher voltages) relative to the steady-state function for sodium. This indicates that as a neuron is depolarized, the sodium current will activate first and then, after a short delay, the potassium current will activate. This delay is where the term 'delayed rectifier potassium current' is from. In effect, this delay controls the shape of the action potential: without a delay the action potential will appear quasi-sinusoidal, but with a delay the action potential will have its generic 'spikiness'. Of course, mathematically, the shape and arrangement of nullclines in the state space are often used to determine if a system is a relaxation oscillator. Throughout this thesis we will vary parameters that affect this delay and in turn see how this

affects synchrony properties.

Figure 2.1(b) shows the activation time constant of the potassium current. The curve is unimodal with a maximum value of $\frac{1}{\epsilon_i}$ (the curve was plotted with $\epsilon = 0.01$, hence a maximum of 100). The value of $\tau(v_i)$ corresponds to how quickly w will approach its steady-state value w_∞. Therefore shifting $\tau(v_i)$ horizontally can also affect the delay described above.

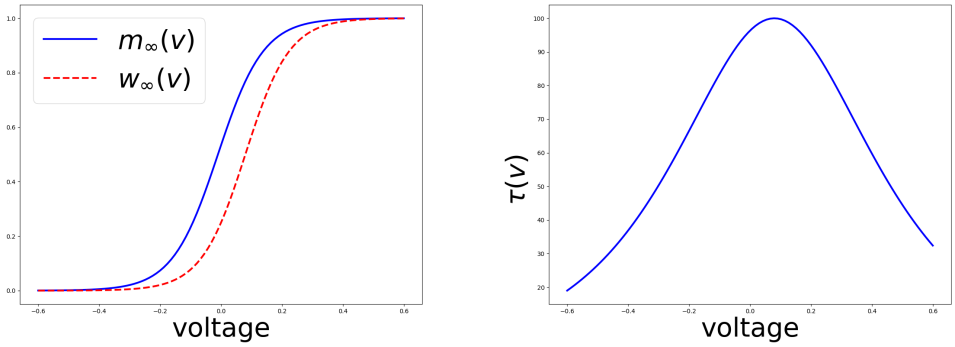

(a) The steady-state functions m_∞ and w_∞ plotted over a relevant voltage domain.

(b) The activation time constant of potassium current plotted over a relevant voltage domain.

Figure 2.1. Plots of (a) steady-state functions and (b) the activtion time constant for K^+.

2.2 Synaptic Current

In (2.1), the term I_{syn} represents the synaptic current. All synapses in this thesis are excitatory, i.e. their effect is to depolarize the postsynaptic neuron. If we consider the i-th neuron, then the incoming synaptic current is given by (2.9).

$$I_{syn,i} = (v_i - v_{syn}) \sum_{j \neq i} \bar{g}_{syn,j} s_j \tag{2.9}$$

Here $\bar{g}_{syn}$ is the maximal conductance of the synapse, s_j is the synaptic variable for the j-th neuron and the summation is taken over all neurons that are connected to the i-th neuron. The synaptic variable s represents the proportion of synaptic channels that are open and is controlled by (2.10).

$$\frac{\mathrm{d}s}{\mathrm{d}t} = \alpha_s(1-s)H_\infty(v-\theta_v) - \beta_s s \tag{2.10}$$

The first term describes the probability that closed channels will open, and the second term describes the probability that open channels will close. Therefore β_s determines the rate of closing, while $\alpha_s H_\infty(v-\theta_v)$ determines the rate of opening [3]. H_∞ is another sigmoidal function whose input is the presynaptic neuronal voltage and is given in (2.11), for a plot of H_∞ refer to Figure 2.2.

$$H_\infty(v) = \frac{1}{1+\exp\left(-\dfrac{v}{\sigma_s}\right)} \tag{2.11}$$

If we view a sigmoidal function as an on/off switch, then this figure tells us that the synaptic variable s is largest when an action potential has occurred (in the presynaptic neuron) and is close to zero when the presynaptic neuron is at (or near) its resting potential.

2.3 Plasticity

In chapter 4, we consider a network that has plastic synapses. The type of plasticity that we implement is called spike-timing dependent plasticity (STDP). STDP comes in a variety of forms [15], so we implement what is perhaps the most common type. Roughly speaking, this rule states that the closer together (in time) that the spikes of a presynaptic and postsynaptic neuron are, then the greater the change in the synaptic conductance from the presynaptic to postsynaptic neuron. Specifically the modeling follows [8] and experimental evidence for this type of modelling can be found in [6, 7]. If the i-th neuron spikes at a time t_i, and the j-th neuron spikes at a

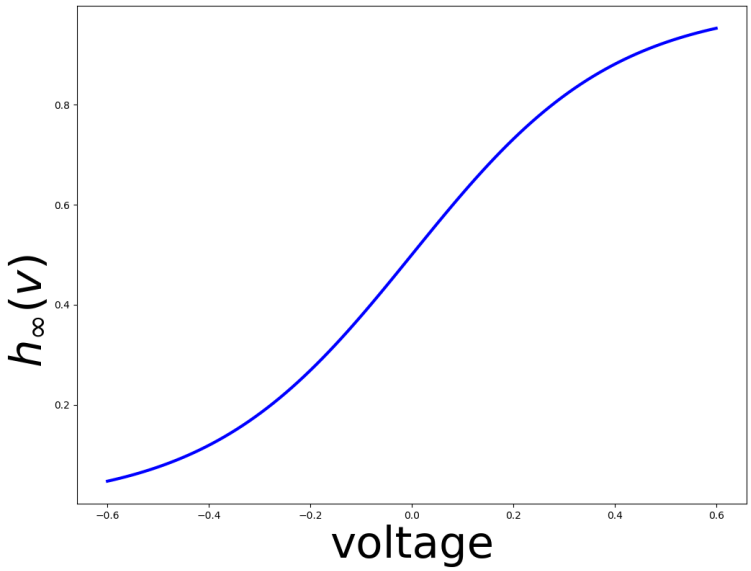

Figure 2.2. $H_\infty(v)$ plotted over a relevant voltage domain.

time t_j, then the conductance of the synapse from the i-th neuron to the j-th neuron is additively updated by the amount given in equation (2.12).

$$\Delta g_{syn} = \text{sgn}(\Delta t) A \exp\left(-k|\Delta t|\right) \tag{2.12}$$

here $\Delta t = t_j - t_i$. Simultaneously, the synaptic conductance from the j-th neuron to the i-th neuron is updated by $-\Delta g_{syn}$. The nature of this update rule is shown below in Figure 2.3. From this figure we can see that the conductance from the pre- to postsynaptic neuron is positively increased if the presynaptic neuron fires before the postsynaptic neuron. The magnitude of the update increases exponentially the closer the firing times. Similarly, the conductance from the pre- to postsynatic neuron is negatively increased if the presynaptic neuron fires after the postsynaptic neuron. From Figure 2.3 it is clear that our update rule is symmetric with respect to time, however this need not be the case, depending on the type of neuron that one is modeling [15].

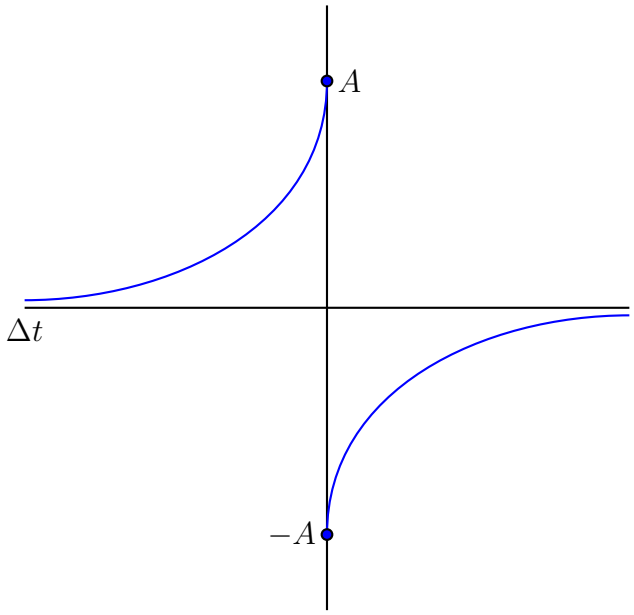

Figure 2.3. STDP update rule plotted as a function of time, Δt.

2.4 Noise

There are various sources of noise present in the nervous system [9, 19, 23]. Here we consider two ways of adding channel noise to the ML model, as described in [10].

2.4.1 Multiplicative Noise

To account for the inherent stochasticity of the potassium ion channels, we add a zero-mean Gaussian white noise term, $\xi(t)$, to the potassium gating variable w in equation (2.4). Hence the potassium current is now given by (2.13). The rest of the neuronal model described in sections 2.1 and 2.2 remains the same.

$$I_K = g_K(w + \xi(t))(v - v_K) \tag{2.13}$$

Inserting (2.13) into (2.1) we obtain the following Langevin-type voltage equation.

$$\frac{\mathrm{d}v}{\mathrm{d}t} = A(v) + B(v)\xi(t) \tag{2.14}$$

$A(v)$ and $B(v)$ are given below.

$$A(v) = -I_{Na} - I_L - I_{syn} + I_{app} - g_K w(v - v_K) \tag{2.15}$$

$$B(v) = -I_{Na} - I_L - I_{syn} + I_{app} - g_K \xi(t)(v - v_K) \tag{2.16}$$

2.4.2 Additive Noise

We also simulate the neurons with a current noise instead of a conductance-based noise. This is a simpler, but perhaps more naive, approach to modeling channel noise than that described above. For example, one drawback is that since the ion channels are voltage-gated, the stochastic process should probably depend not only on time, but also on the membrane voltage [10]. However, the exact dependence on voltage may not be known. The only change to the neuronal model described in sections 2.1 and 2.2 is that equation (2.1) now has an additive zero-mean Gaussian white noise term, $\xi(t)$. Here $\xi(t)$ is also meant to model the stochastic nature of the ion channels in the neuron's membrane [10]. The new voltage equation is given in (2.17).

$$\frac{\mathrm{d}v}{\mathrm{d}t} = -I_{Na} - I_K - I_L - I_{syn} + I_{app} + \xi(t) \tag{2.17}$$

2.5 Network Model

Throughout this thesis we utilize a simple neural network consisting of two neurons coupled via unidirectional excitatory synapses, see Figure 2.4. The two neurons have a slightly different firing rate, i.e. their respective ϵ values differ slightly (cf. section 2.6). The initial value of the maximal synaptic conductance is $g_{syn} = 0.005$, so that the coupling is weak. This heterogeneity and weak synaptic coupling ensures that synchrony between the two neurons is present, but is relatively weak.

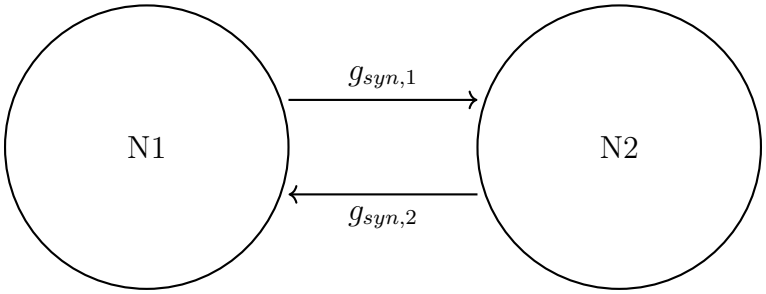

Figure 2.4. Schematics of the network: two neurons coupled with mutually excitatory synapses.

2.6 Parameter Values

The cellular and synaptic parameter values used are given in Table 2.1. These are the same parameter values that were used in [11]. The plastic parameters will be given in section 4.1, and the stochastic parameter is given in section 6.1.

Table 2.1.
List of cellular and synaptic parameter values.

$g_{Na} = 1$	$g_K = 3.1$	$g_L = 0.5$	$v_{NA} = 1$	$v_K = -0.7$	$v_L = -0.4$
$v_{m1} = -0.01$	$v_{m2} = 0.15$	$v_{w1} = 0.08$	$\beta = 0.145$	$I_{app} = 0.045$	$\epsilon_1 = 0.02$
$\epsilon_2 = 1.2\epsilon_1$	$v_{syn} = 0.5$	$\alpha_s = 2$	$\beta_s = 0.2$	$\theta_v = 0.0$	$\sigma_s = 0.2$

3. SYNCHRONIZATION METHODS AND ANALYSIS

Detection of synchronized dynamics within the network follows the time-series methods outlined in [11, 12]. The experimental studies mentioned in section 1.4 made use of a similar analysis. The reason for a similar, but not identical, analysis stems from the experimental nature of the data. For instance, in [14] the data was collected via electroencephalograms (EEGs). This represents a collective signal from a large number of neurons, as opposed to the system of two neurons in this modeling study. Naturally their recorded signal is capable of much more complex dynamics than are possible in our system. Other key differences include filtering the signal to certain frequency bands of interest, and reconstructing the phase using the Hilbert transform. As described below, we use a more geometric definition of the phase because we have access to all the state variables, and it is also computationally less expensive. We outline the procedure below in detail.

3.1 Phase and Averaged Synchrony Strength

We use a phase-locking definition of synchrony. The phase, $\phi(t)$, of a neuron is defined geometrically as in (3.1).

$$\phi(t) = \arctan\left(\frac{v(t) - \hat{v}}{w(t) - \hat{w}}\right) \tag{3.1}$$

Here $(\hat{w}, \hat{v})$ is an arbitrary point within the neuron's limit cycle in the $(w, v)-$plane. The implementation of (3.1) in Python used numpy's arctan2 function. This allows the phase to be defined over the entire closed interval $[-\pi, \pi]$; in particular, it allows $w(t) - \hat{w} = 0$.

Once the phase of each neuron within the network has been computed, an average synchrony strength can be calculated, as in (3.2). This index is often referred to as the mean phase coherence.

$$\gamma = \left| \frac{1}{N} \sum_{j=1}^{N} e^{i\Delta\phi(t_j)} \right|^2 \tag{3.2}$$

where $\Delta\phi(t_j) = \phi_1(t_j) - \phi_2(t_j)$ is the difference of the phases of neurons 1 and 2 at time t_j. N is the number of data points. The value of γ is bounded between 0 and 1, where the former represents a complete lack of synchrony and the latter represents perfect synchrony.

For the following procedure to be applicable, the network must have a synchronized state [12]. This means there should be some degree of phase-locking present, i.e. there is a preferred value of the phase difference $\Delta\phi$. A preliminary way to check this would be to simply plot the histogram of phase differences. A more analytical method would be to compare the synchrony strength γ to some chosen significance value [12]. As will be seen in the sections below, the necessity of having a synchronized state lies in the fact that we will be detecting when the phase variable leaves, and subsequently, re-enters the synchronized state.

3.2 Stroboscopic Map

The synchrony strength γ represents an average value of phase-locking over the time interval $[t_1, t_N]$. Yet to describe the pattern of synchrony within a system, one needs to look at the transitions to and from the synchronized state. This is best done on shorter time scales to give a better temporal resolution. The methodology in the next couple paragraphs develops a definition of synchrony on a single cycle of oscillation time scale.

To accomplish this we construct the points within a stroboscopic map. Specifically, we view ϕ_1 when it increases past zero, say at time t_j, and record the value of $\phi_2(t_j) \equiv \Phi_j$. This generates a sequences of numbers $\{\Phi_j\}_{j=1}^{M}$. Due to the existence of some level of phase-locking, there is a clustering of points around some phase value, say $\tilde{\Phi}$. To find this point numerically, we create a histogram of Φ_j with 10 bins. Then we take the center of the bin with the highest population as $\tilde{\Phi}$. An illustration of the strobscopic map is given below in Figure 3.1. Here it can be seen that $\tilde{\Phi}$ is close to $-\pi$.

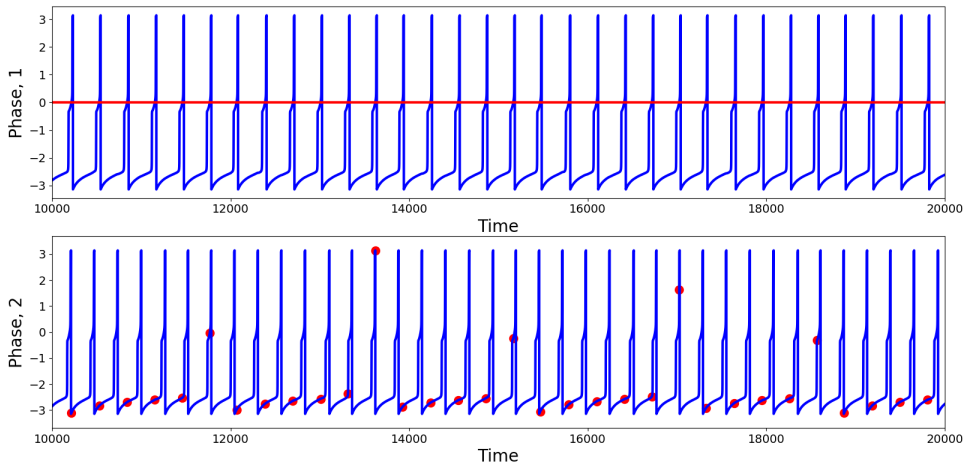

Figure 3.1. Top: phase variable for neuron 1. The horizontal line is when ϕ_1 increases past zero. Bottom: phase variable for neuron 2. The points indicate the values of Φ_j. $\epsilon_1 = 0.005$, the rest of parameter values given in section 2.6.

We will say the system is in a desynchronized state when a point Φ_j in the stroboscopic map differs from the preferred phase value of $\tilde{\Phi}$ by more than $\frac{\pi}{2}$. Otherwise the system is said to be in a synchronized state. As can be seen in Figure 3.1 there are several sequences of 4–5 points where the phase of neuron 2 is relatively constant. During these cycles, the system would be considered in synchrony. In between the synchronized states the phase of neuron 2 deviates considerably from $\tilde{\Phi}$, hence during

these cycles the system is in a desynchronized state. We note that the choice of $\frac{\pi}{2}$ is arbitrary, yet convenient in that it will partition the $(\Phi_j, \Phi_{j+1})-$space into quadrants. The choice of $\frac{\pi}{2}$ was also used in the previous studies using experimental data (cf. section 1.4).

3.3 Phase Space and Lengths of Desynchronization Events

We now translate our definition of synchrony to the $(\Phi_j, \Phi_{j+1})-$space. To do this we take our sequence $\{\Phi_j\}_{j=1}^{M}$ and plot the points (Φ_j, Φ_{j+1}) for $j = 1, \ldots, M-1$. Synchrony will present itself as a grouping around the diagonal $\Phi_j = \Phi_{j+1}$, i.e. when the future phase is close to the current phase. Naturally this can happen in either the first or the third quadrant, so for consistency we shift the center of the grouping to the center of the first quadrant, i.e. to $\left(\frac{\pi}{2}, \frac{\pi}{2}\right)$. Since the phase space is $[-\pi, \pi] \times [-\pi, \pi]$ (a torus), this can be accomplished by translating $\{\Phi_j\}$ an appropriate amount and then taking that modulo 2π. An illustration of the sequence $\{\Phi_j\}$ before and after the shift is given in Figure 3.2.

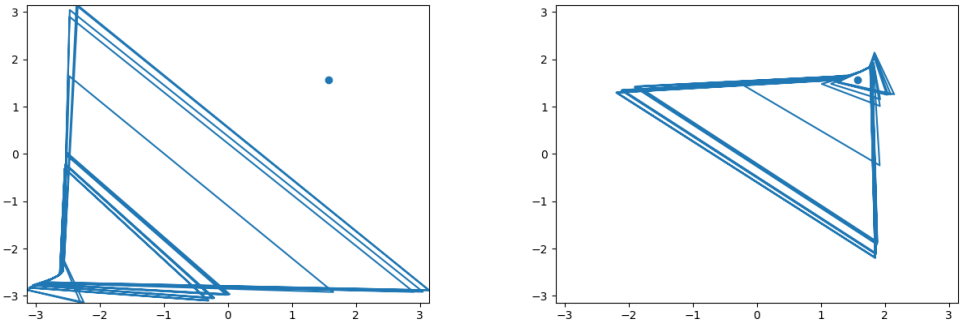

(a) Stroboscopic map before shifting.

(b) Stroboscopic map after shifting.

Figure 3.2. The point in the first quadrant is at $\left(\frac{\pi}{2}, \frac{\pi}{2}\right)$. $\epsilon = 0.005$, the rest of parameters as given in section 2.6.

The phase space is naturally partitioned into four quadrants (due to our definition of synchrony from the previous section). Since the preferred phase angle $\tilde{\Phi}$ has been shifted to the center of the first quadrant, we label this quadrant as the region where the system is in a synchronized state. The remaining three quadrants are labeled as the regions where the system is in a desynchronized state.

To study the dynamics of the system in the phase space, we need to understand how the system can transition from one region to another. Since the second coordinate of each point in the phase space is the future phase, only some transitions are possible. Figure 3.3 shows all possible transitions between regions. Notice that the regions are numbered in a clockwise fashion because the direction of the dynamics is primarily in this direction.

We now define the length of a desynchronization event to be the number of cycles that the system spends outside the synchronization region (quadrant 1). This can be rephrased as the number of points (Φ_j, Φ_{j+1}) outside the first qudrant minus one. The shortest possible desynchronization event is length one; the system spends one cycle in the desynchronization region. This is illustrated in 3.4(a). Length two is the next shortest possible desynchronization event, this is illustrated in 3.4(b). For both length one and length two events there is only one possible trajectory (those shown in Figure 3.4). Length three and higher events have multiple possible trajectories.

An illustration of different desynchronization durations and dynamics with different modes of desynchronizations is provided in Figure 3.5. Voltages and distributions of desynchronization durations for mode one dynamics are in the left column, the ones for mode two dynamics are in the right column. The synchronization is not perfect, and synchronized dynamics (i.e. the phase difference is close to the preferred one) are interspersed with desynchronized intervals. Note that the preferred phase difference

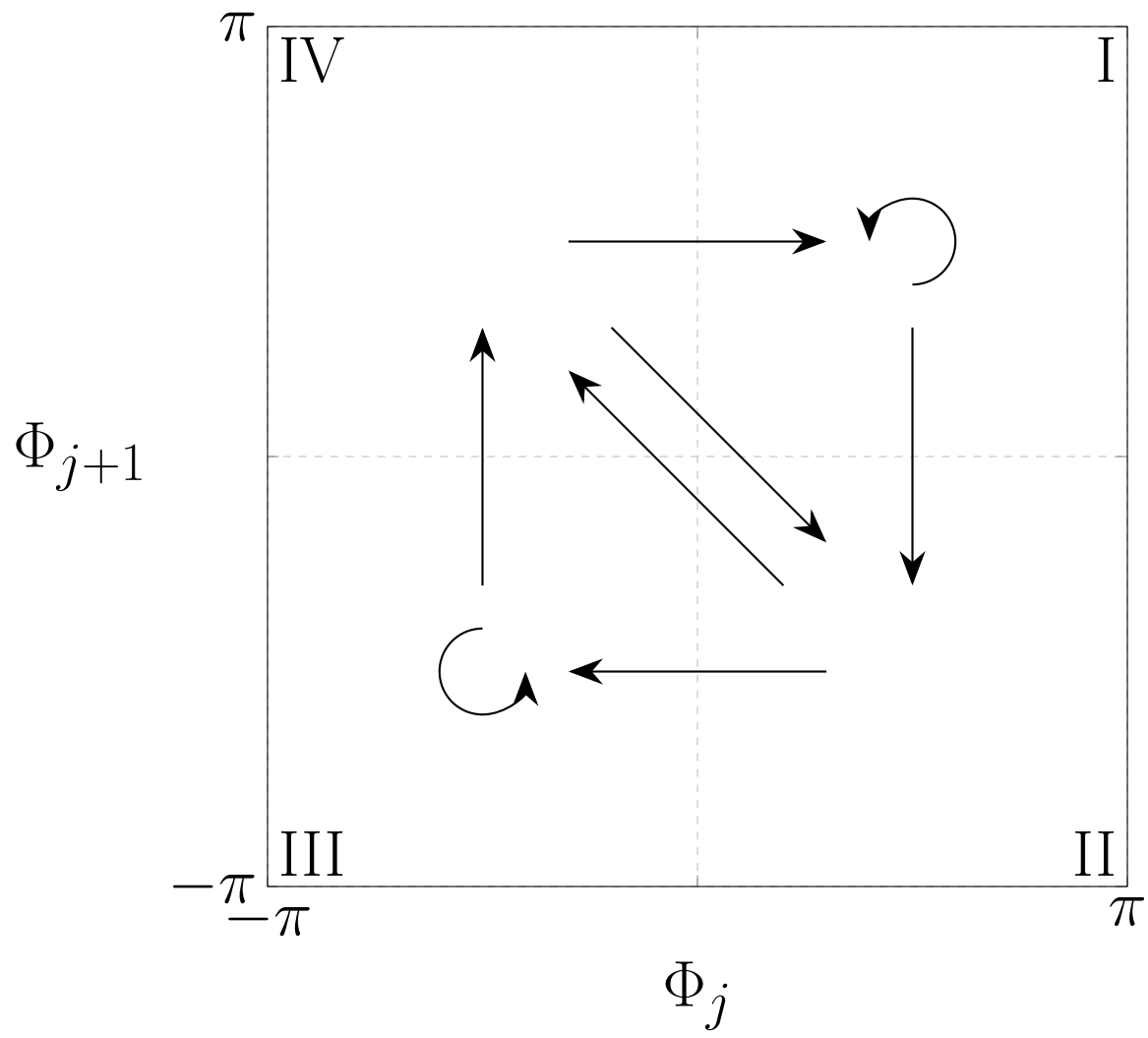

Figure 3.3. Diagram illustrating all possible transitions between quadrants in the $(\Phi_j, \Phi_{j+1})-$space. Beginning of the arrow indicates quadrants that the system starts in, arrowhead indicates quadrant that the system ends in. Adapted from [14].

is not necessarily zero, so the zero-lag state is not necessarily a synchronized state.

During the numerical simulation of a system we record the lengths of all desynchronization events and then reconstruct the distribution of these durations. We characterize a system's temporal patterning of synchrony by taking the mode of this

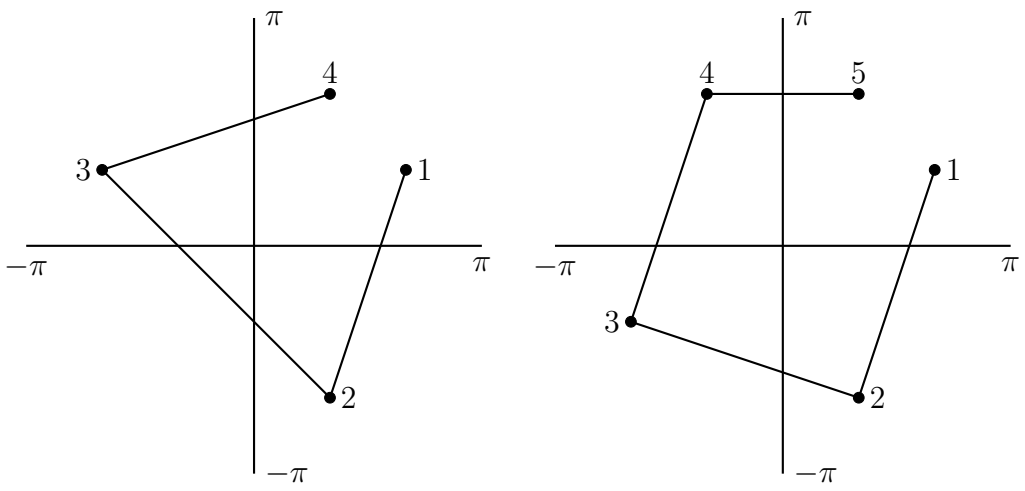

(a) Length one desynchronization event. (b) Length two desynchronization event.

Figure 3.4. Illustrations of two desynchronization events.

distribution. For later reference, we call a system "mode n" if the mode of the lengths of all desynchronization events is n. Therefore a mode one system has more length one desynchronization events than any other length; the synchronized dynamics are interrupted by predominantly short desynchronizations. The larger the mode, the more likely it is for a system to experience longer desynchronizations.

In closing, there are two items to mention. First, the lengths of desynchronization events are measured in number of cycles of oscillations of a neuron, *not* in absolute time units. This allows one to compare systems that have different frequencies. Second, the synchrony strength γ can be independent of the mode of the system. That is, a mode one system and a mode four system could have the same amount of overall synchrony. This is because it is not just the lengths of the desynchronization events that affect the synchrony strength, but also the number of such desynchronization events.

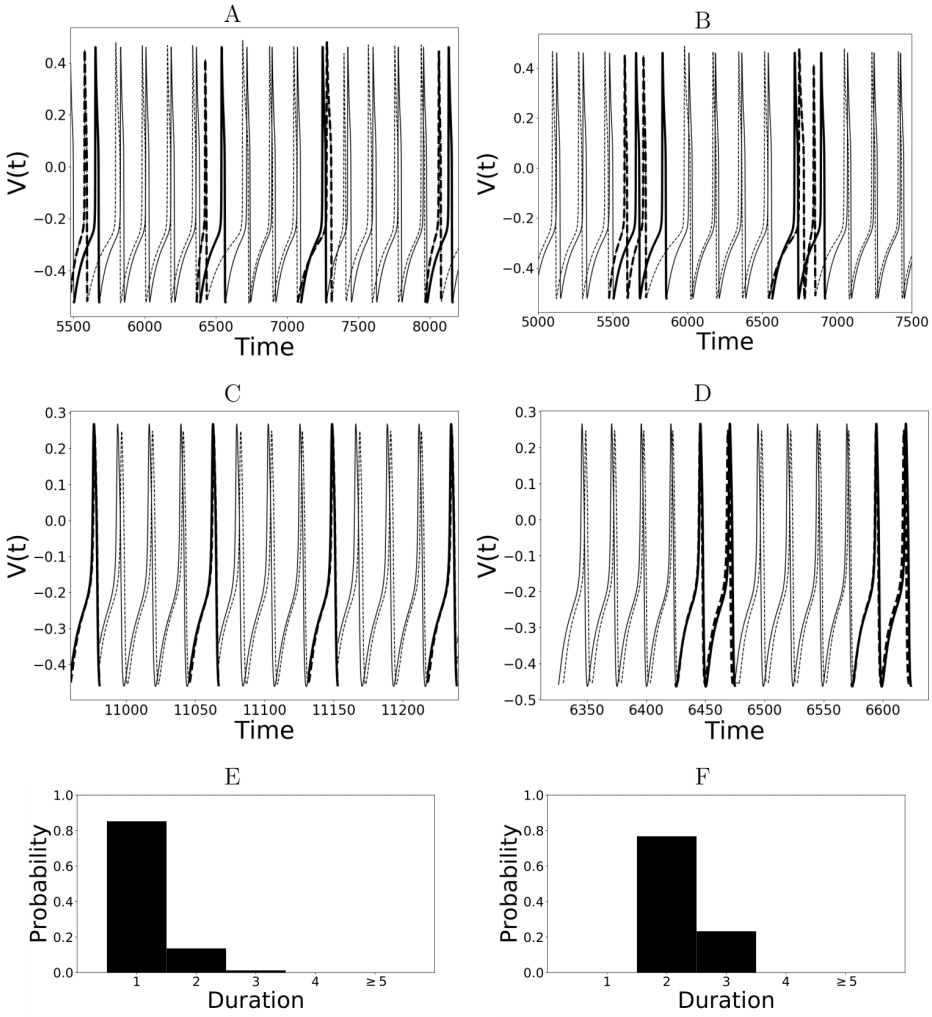

Figure 3.5. Illustration of mode one and mode two dynamics. A—D depict voltage traces of two partially synchronized neurons (solid and dashed lines). When the phase difference is close to the preferred phase difference the voltage traces are thin lines indicating proximity to a synchronized state. When the phase difference is not close to the preferred one, the lines are thick to indicate the desynchronizations. A and C illustrate short desynchronizations (lasting one cycle of oscillation), B and D show longer desynchronizations (lasting two cycles of oscillation). A and B are artificially generated examples, while C and D are examples generated by the network considered in the section below. In a longer time-series, the desynchronizations of different durations may coexist, however, usually one duration will prevail. The distributions showing relative frequency of different desynchronizations for the dynamics with predominantly short desynchronizations (like A and C) and with longer desynchronizations (like B and D) are presented in E and F respectively. We see the first column represents mode one dynamics while column two represents mode two dynamics.

4. DESCRIPTION OF PARAMETERS AND PREVIOUS RESULTS

The focus of this chapter is to:

1. briefly introduce the reader to previous results from [11] where the neural model is both non-plastic and non-noisy. This will allow the reader to better understand the results given in chapters 5 and 6.

2. explain the effect that varying certain cellular parameters has on the relative timing of the sodium and delayed-rectifier potassium currents during the course of an action potential.

The neural network is as described in section 2.5 with parameter values given in section 2.6. Both neurons in the network are mathematically described by equations (2.1)-(2.11). For a given set of parameter values, we numerically solve the system of differential equations. Then we calculate the mode of desynchronization durations, the synchronization strength γ, and the mean firing frequency of the neurons. In the sections below, each cellular parameter that is varied affects the timing of the delayed-rectified potassium current. The effect of each parameter will be described in detail. Note that all the figures in this chapter are recreations of the results from [11], and while there are minor differences (due to numerical implementations) the figures are qualitatively the same.

4.1 Effect of the Peak Value of the Activation Time Constant (i.e. ϵ)

Recall from (2.8) that $\tau(v) \propto \frac{1}{\epsilon}$, indeed the global maximum of the activation time-constant τ is $\frac{1}{\epsilon}$. Hence as ϵ is increased, τ decreases across its entire domain, see Figure 4.1. The effect of decreasing τ is to accelerate the activation of potassium

current because $\frac{dw}{dt} \propto \frac{1}{\tau(v)}$ (see (2.2)). In summary, a larger value of ϵ acts to speed up the activation of potassium current, while a smaller value of ϵ delays the activation of potassium current. The effect of different values of ϵ on the shape of the action potential is seen in Figure 4.2. In 4.2(a) the value of ϵ is quite small and we see that the action potential has generic spikiness; a very quick up- and down-stroke. Whereas in 4.2(b) the value ϵ is much larger and the action potential is more quasi-sinusoidal. We also note that if we compare the scales on the horizontal axes in Figure 4.2 we see that the firing frequency increases as ϵ increases, this is simply because the rate of change of w is proportional to ϵ.

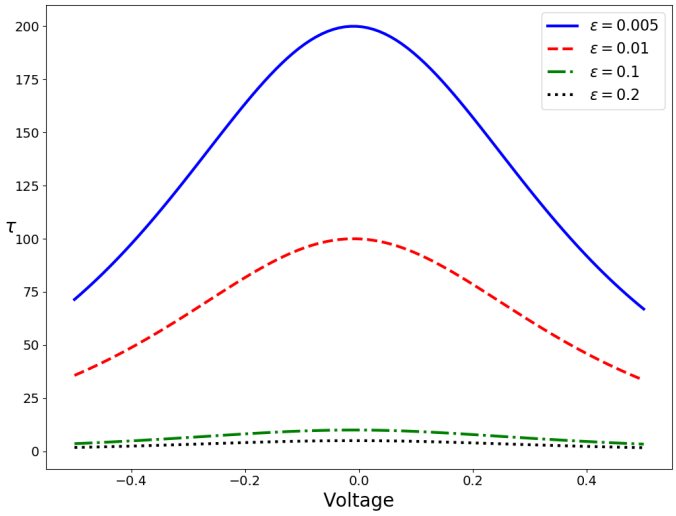

Figure 4.1. The activation time-constant $\tau(v)$ for potassium current plotted over a relevant voltage domain.

As the ϵ value of each neuron in the system increases, the pattern of synchronization changes as shown in Figure 4.3. In 4.3(a) we see that small ϵ values promote mode one dynamics, while larger ϵ values promote modes greater than one. This indicates that a delayed potassium current tends to promote short desynchronization events, while a potassium current that activates sooner tends to promote longer

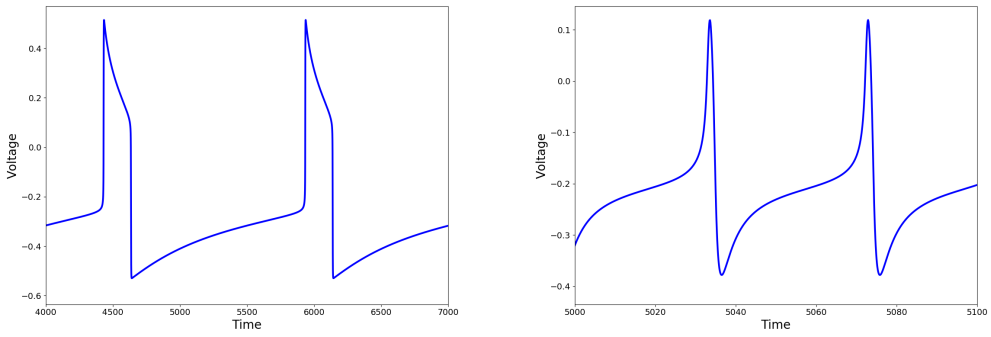

(a) $\epsilon = 0.001$ (b) $\epsilon = 0.5$

Figure 4.2. Simulation of isolated ML neuron with different ϵ values.

desynchronization events. In 4.3(b) we see that the synchrony strength γ is relatively constant, hence we may conclude that systems with inherently different dynamics (i.e. different modes) may yet have the same synchrony strength on the average. As will be seen throughout the following results, γ and the mode will sometimes vary with each other, and sometimes they are independent (as they are here). This independence has also been observed in studies on experimental data, e.g. [44]. 4.3(c) shows the increase in frequency as ϵ increases.

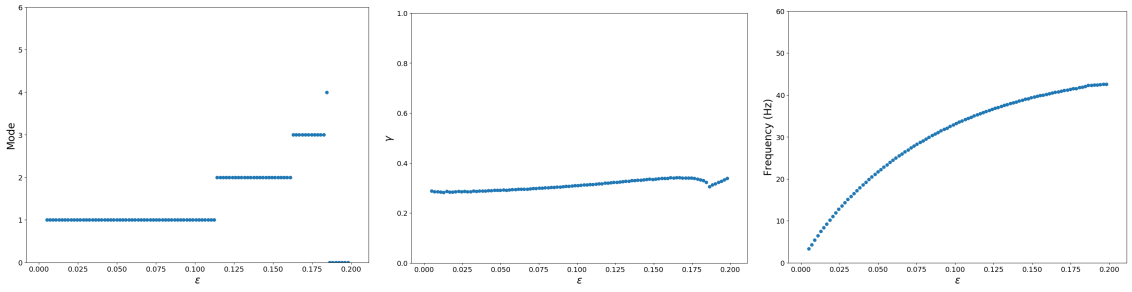

(a) Mode of system. (b) Synchrony strength γ. (c) Mean firing frequency.

Figure 4.3. Effect of varying ϵ_1 and ϵ_2.

4.2 Effect of the Width of the Activation Time Constant (i.e. β)

We remind the reader that β appears in the equation for $w_\infty(v)$ ((2.7), a sigmoidal function), and in the equation for $\tau(v)$ ((2.8), a unimodal function). As β increases, the derivative of w_∞ evaluated at its half-height ($v = 0$) decreases and the width of the peak of τ decreases. These effects are illustrated in 4.4. The result of these effects is to delay the activation of potassium current because $\frac{\mathrm{d}w}{\mathrm{d}t} \propto \frac{1}{\tau(v)}$.

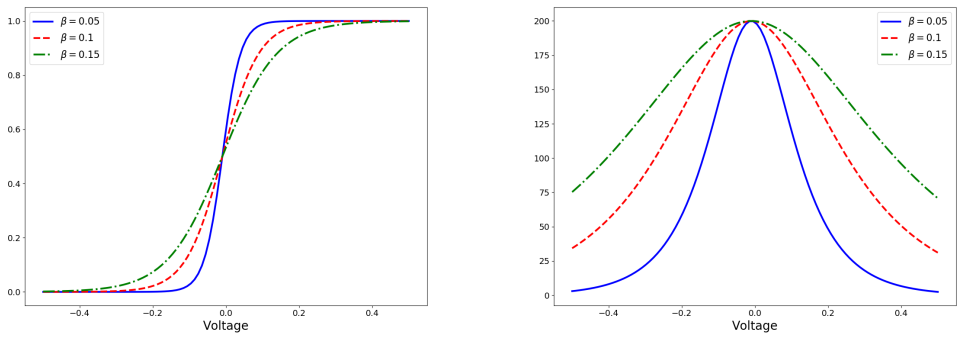

(a) (b)

Figure 4.4. Effect of β on activation of potassium current. In (a) we see the steady-state value $w_\infty(v)$, with v_{w1} fixed, plotted over a relevant voltage domain. In (b) we see the activation time-constant $\tau(v)$, with fixed ϵ and v_{w1}, plotted over a relevant voltage domain.

As the value of β in the system increases, the pattern of synchroniztion changes as shown in Figure 4.5. In 4.5(a) we see that small β values promote modes greater than one, while a larger β value will promote mode one dynamics. Hence a delayed potassium current tends to promote shorter desynchronization events, while a potassium current that activates faster tends to promote longer desynchronization events. In 4.5(b) we see that as the mode of the system increases, the synchronization strength γ decreases. The mean firing frequency of the system decreases as β increases because $\frac{\mathrm{d}w}{\mathrm{d}t} \propto \frac{1}{\tau(v)}$, see 4.5(c).

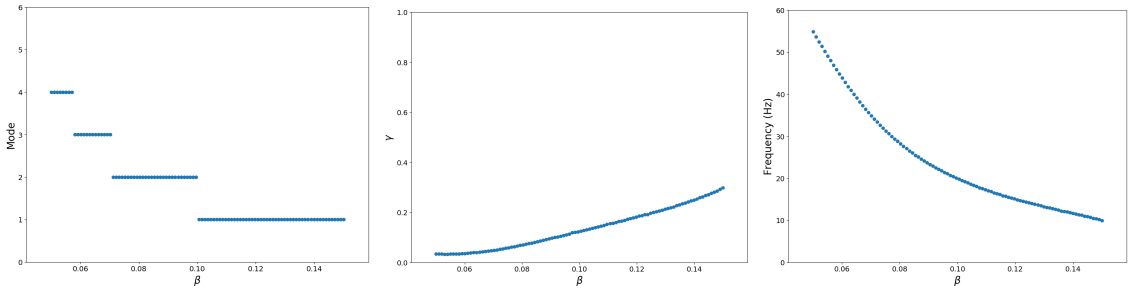

(a) Mode of system. (b) Synchrony strength γ. (c) Mean firing frequency.

Figure 4.5. Effect of varying β.

4.3 Effect of the Voltage of Half Activation and Maximal Activation for the Activation Time Constant (i.e. v_{w1})

The parameter v_{w1} appears in the equation for $w_\infty(v)$, (2.7), and in the equation for $\tau(v)$, (2.8). As can be seen in Figure 4.6, the result of varying v_{w1} is to affect a horizontal translation in both the w_∞ and τ functions. Specifically, as v_{w1} is increases, both functions are shifted towards higher voltage values. As v_{w1} varies, the amplitude of the action potentials remains relatively constant, i.e. the voltage range that the neuron operates within remains relatively constant; roughly in the interval $[-0.5, 0.4]$. Therefore as the functions w_∞ and τ are shifted towards higher voltages, their values decreases over this voltage interval which causes potassium current to activate sooner because $\frac{\mathrm{d}w}{\mathrm{d}t} \propto \frac{1}{\tau(v)}$.

As the value of v_{w1} in the system increases, the pattern of synchronization changes as shown in Figure 4.7. In 4.7(a) we see that small v_{w1} values promote mode one dynamics, while larger v_{w1} values will promote modes greater than one. In terms of the potassium current, this means that a delayed potassium currents tends to promote dynamics with shorter desynchronizations, while a potassium current that activates quicker promotes dynamics that tend towards longer desynchronization events. In 4.7(b) we see that systems with smaller modes are associated with a higher synchro-

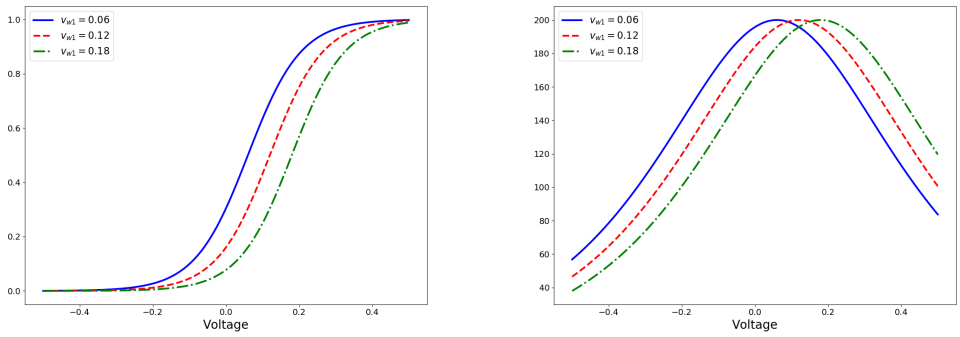

(a) (b)

Figure 4.6. Effect of v_{w1} on activation of potassium current. In (a) we see the steady-state value $w_\infty(v)$, with β fixed, plotted over a relevant voltage domain. In (b) we see the activation time-constant $\tau(v)$, with fixed ϵ and β, plotted over a relevant voltage domain.

nization strength γ, while in 4.7(c) we see that the mean firing frequency of the system is relatively constant with respect to v_{w1}.

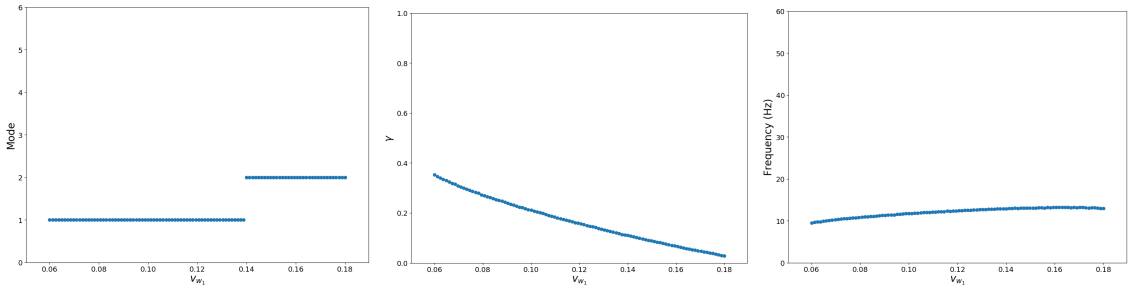

(a) Mode of system. (b) Synchrony strength γ. (c) Mean firing frequency.

Figure 4.7. Effect of varying v_{w1}.

4.4 Effect of Simultaneous Changes in β_w and β_τ

In Figure 4.5 we saw that the variation of β induced a change in the mode of the system as well as a change in both the synchrony strength γ and the frequency of the

system. If we take the parameter β and split it into two independent parameters, β_w and β_τ, it is possible to affect the mode of the system while maintaining a constant synchrony strength γ and frequency. We modify equations (2.8) and (2.8) as:

$$w_\infty(v) = \frac{1}{1 + \exp\left(-2\dfrac{v - v_{w1}}{\beta_w}\right)} \tag{4.1}$$

$$\tau(v) = \frac{2}{\epsilon\left(\exp\left(\dfrac{v - v_{w1}}{2\beta_\tau}\right) + \exp\left(\dfrac{v_{w1} - v}{2\beta_\tau}\right)\right)}. \tag{4.2}$$

The effect of β on the activation of potassium current is now also split: β_w controls the slope at the half-height of the steady-state value w_∞ while β_τ controls the width of the peak of the activation time-constant τ.

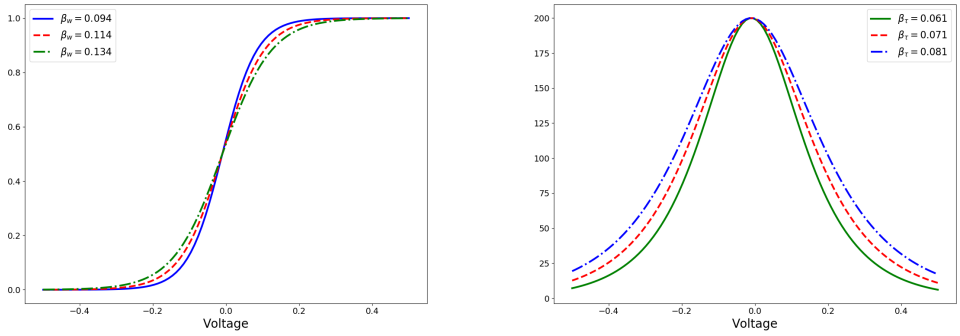

(a) (b)

Figure 4.8. Effect of varying β_w and β_τ on activation of potassium current. In (a) we see the steady-state value $w_\infty(v)$, with v_{w1} fixed, plotted over a relevant voltage domain. The activation time-constant $\tau(v)$, with fixed v_{w1} and ϵ, plotted over a relevant voltage domain.

As β_w and β_τ are varied in opposing directions (one increases while the other decreases), the pattern of synchronization changes as seen in Figure 4.9. In 4.9(a) we see that a small β_w and a larger β_τ promotes mode one dynamics, and as β_w is increased and β_τ is simultaneously decreased the mode of the system grows. In 4.9(b)

and 4.9(c) the synchrony strength γ and the mean firing frequency is held relatively constant, which was the desired effect.

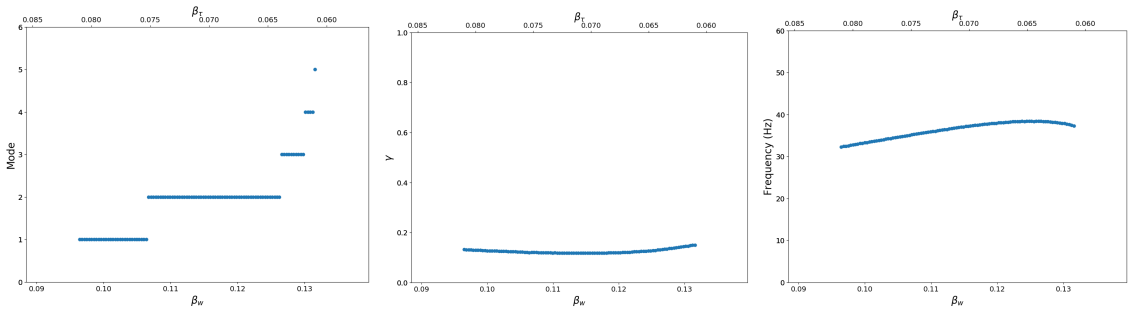

(a) Mode of system. (b) Synchrony strength γ. (c) Mean firing frequency.

Figure 4.9. Effect of varying β_w and β_τ.

5. PLASTIC MODEL

In this chapter we implement a neural network consisting of two neurons connected via excitatory synapses with spike-timing dependent plasticity (STDP), as described in chapter 2. STDP is a common neural phenomenon [16] that, among other things, can lead to an enhancement of neural synchrony [17, 18]. In the following sections we provide evidence that STDP may affect not only the overall synchrony strength γ, but also the temporal patterning of the synchronization. In particular, we show that there are regions of the parameter space where STDP will drive the system to be mode one, i.e. STDP will tend to promote short desynchronization dynamics. The non-plastic variant of this system is discussed in chapter 4.

5.1 Numerical Implementation

The system of differential equations was solved numerically in Python using the built-in odeint function from the SciPy module (v.1.4.1). This function implements either the Adams method or a backward differentiation formula (BDF) method depending on the stiffness of the problem. The solution was reported at multiples of the time step $dt = 0.1$ (assuming the time units are milliseconds), however the function uses an adaptive step size and there was no lower bound on the length of the intermediate time steps that may be used (similarly, there was no upper bound restriction on the number of intermediate steps that were taken). The absolute and relative tolerances for the method were kept at the default value of 1.49×10^{-8}. While the solution depends on the initial conditions, its statistical properties (such as the firing rate, synchrony pattern characteristics etc...) do not. The initial conditions were $v_{1,0} = 0.1$, $w_{1,0} = 0.376$, $s_{1,0} = 0.86$, $v_{2,0} = -0.29$, $w_{2,0} = 0.127$, $s_{2,0} = 0.64$. These were the same initial conditions as used in the previous study of [11]. The system was

solved on the time interval $[0, 25000]$, the first 20% of the time-series was removed from analysis. The removal of the initial part of the time-series is necessary because we are not interested in the transient behavior of the system before it displays some stationary dynamics (i.e. regular oscillatory behavior).

We remind the reader that there are two plasticity parameters, k and A (cf. section 2.3). The amplitude of the update rule is A, while k represents the reciprocal of the timescale on which the magnitude of the plastic update rule decays exponentially. To explore the parameter space we vary A from 0.0001 to 0.01 using 40 linearly spaced points (endpoints included). k took on the following values: $\{0.01, 0.05, 0.1, 0.3, 0.7, 1, 2, 5, 10, 20, 50\}$. We also vary cellular parameters, hence for each cellular parameter value there are 440 numerical simulations canvasing the region of parameter space described above. To implement plasticity, the integration was paused after each time step and, if necessary, the synaptic strengths were updated according to (2.12). Specifically, the voltage threshold to define an action potential was set at 0.2.

Lastly we mention that the synaptic conductance g_{syn} is bounded below by zero, but there is no upper bound. While the synaptic conductances often display some initial transient behavior (e.g. slow growth or decay or very slow large oscillation), they generally settle down to some stationary variations, see Figure 5.1.

5.2 Results of Plasticity on Synchrony Patterns

5.2.1 Effect of the Peak Value of the Activation Time Constant (i.e. ϵ)

The parameter ϵ was varied from 0.005 to 0.2 using 40 linearly spaced points (endpoints included). However we will only present results from two parameter values that are representative of mode one and mode two dynamics.

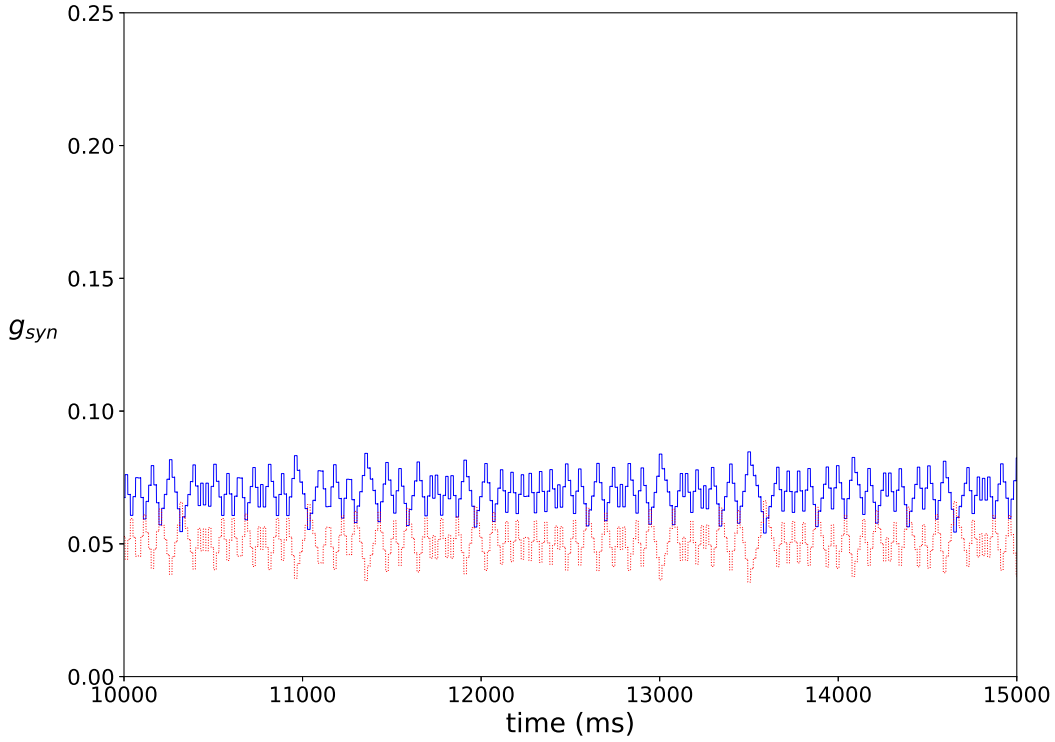

Figure 5.1. An example of a typical temporal evolution of synaptic weights in a network with plasticity ($\epsilon = 0.15, A = 0.009, k = 0.3$). Color and line type distinguish the conductances of the two synapses in the network.

For $\epsilon = 0.05$, the non-plastic system is mode one. Now the non-plastic system is changed to include STDP. The changes in the temporal patterning of synchronization dynamics are illustrated in Figure 5.2. Figure 5.2A is a diagram of the mode of the desynchronization durations in the space of plasticity parameters, A and k. The plasticity effects are negligible across the top (very large k implies a quick decay of the change in synaptic strength), and especially in the upper left corner (large k and a small amplitude A). In these areas the values of the plasticity parameters are such that the magnitude of the update, Δg_{syn}, is negligible (the average update is usually in the interval $[0.0, 10^{-5}]$, on the larger end this corresponds to about 0.2% of the

initial value of g_{syn}. Hence, the plastic system continues to be mode one in these areas.

The rest of the parameter space, in particular the central region, displays a high proportion of mode one dynamics as well. In these areas plasticity is not negligible, as the synaptic strength can vary to a substantial degree. However, even in the presence of STDP, mode one dynamics persist. For the diagram in Figure 5.2A, about 85% of the parameter space points correspond to mode one systems.

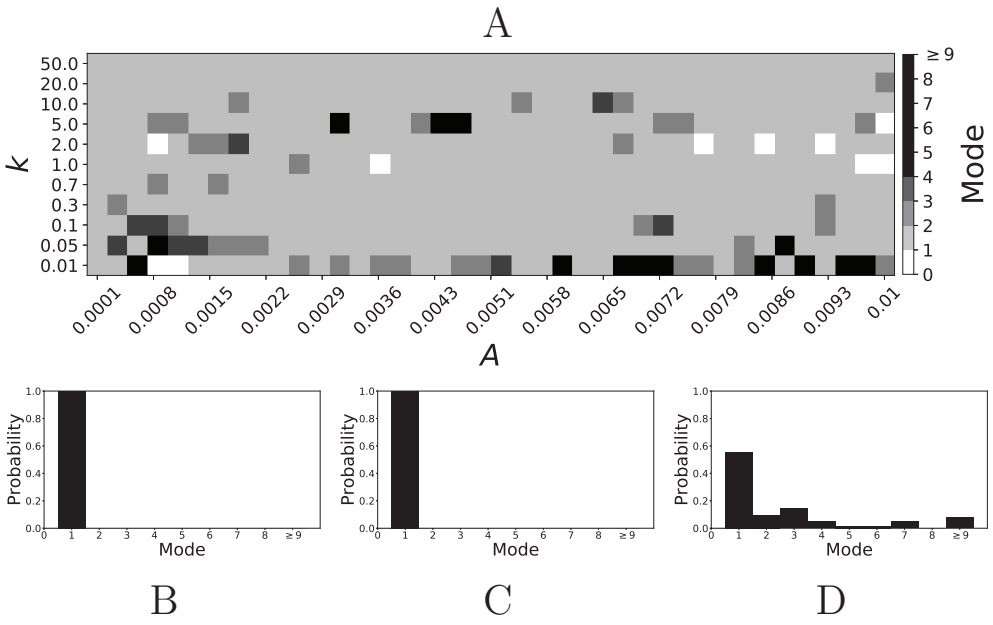

Figure 5.2. A system exhibiting mode one dynamics in the non-plastic case is subjected to plasticity ($\epsilon = 0.05$). A: Mode is colored via gray scale, see legend on the right of the diagram. The amplitude of the synaptic update, A, is varied along the horizontal axis. The reciprocal of the timescale of the synaptic update, k, is varied along the vertical axis. B, C and D show the changes in the histogram of desynchronization durations as plasticity becomes stronger. B: The system without plasticity. C: The system with very weak plasticity: $A = 0.0047, k = 20.0$. D: The system with moderate plasticity: $A = 0.0047, k = 0.05$.

To illustrate the effect of plasticity on a distribution of desynchronization durations, refer to Figure 5.2B, C and D. Plasticity effects increase from left to right. The distribution of durations changes: at a weak level of plasticity the durations are exclusively length one, while at a stronger level of plasticity some longer durations are observed. We note that STDP clearly has a non-zero effect on the system, yet the preponderance of length one desynchronization events is preserved.

Now let us look at the effect of plasticity on the dynamics in systems with a mode larger than one. We consider $\epsilon = 0.15$. The non-plastic system is mode two (the synchronization index γ is virtually unchanged from that of $\epsilon = 0.05$, although the frequency of oscillations increases by several times [11]). Mode two means the desynchronizations tend to be longer than those of the mode one case.

Figure 5.3 shows the effect of STDP on the system that is mode two in the non-plastic case. As explained earlier, the plasticity effects are negligible across the top of Figure 5.3A, and especially in the upper left corner. We note that this region of the parameter space exhibits mode two dynamics (as expected). However, throughout the entire parameter space it is seen that a majority of parameter values correspond to mode one systems (the large central region in Figure 5.3A). Overall, about 20% of the parameter space points stay mode two, while over 65% exhibit mode one dynamics (and less than 15% correspond to larger than mode two systems).

To illustrate the effect of plasticity on the distribution of desynchronization durations, refer to Figure 5.3B, C and D. Plasticity effects increase from left to right. Here we see that the introduction of weak plasticity can be sufficient to shift the system from mode two to mode one (Figure 5.3C). This means desynchronizations tend to become shorter in the plastic case. At stronger levels of plasticity (Figure 5.3D), the distribution widens, however the vast majority of desynchronization events remain length one.

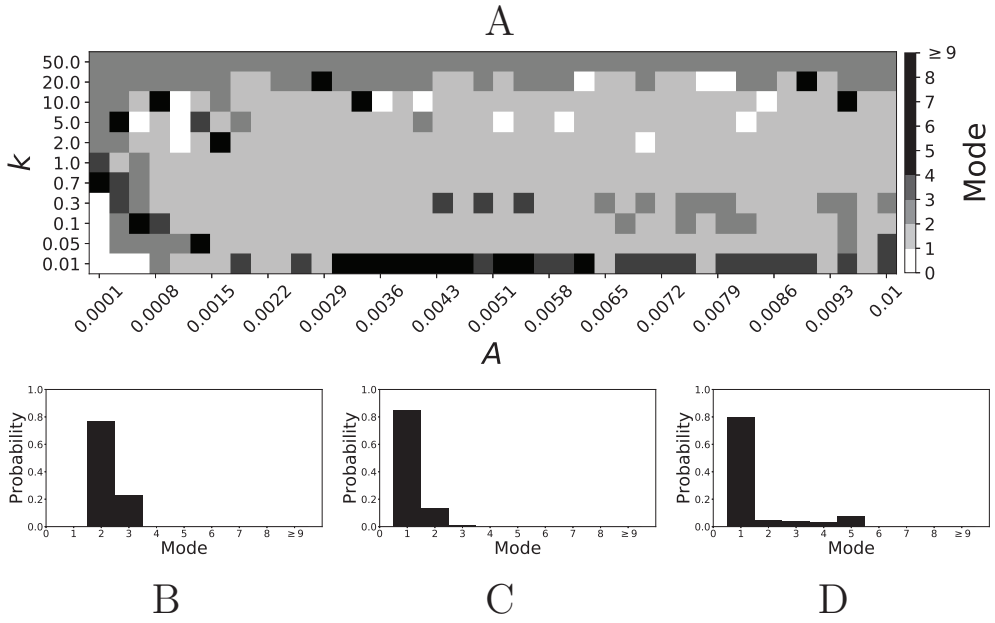

Figure 5.3. A system exhibiting mode two dynamics in the non-plastic case is subjected to plasticity ($\epsilon = 0.15$). A: Mode is colored via gray scale, see legend on the right of the diagram. The amplitude of the synaptic update, A, is varied along the horizontal axis. The reciprocal of the timescale of the synaptic update, k, is varied along the vertical axis. B, C and D show the changes in the histogram of desynchronization durations as plasticity becomes stronger. B: The system without plasticity. C: The system with very weak plasticity: $A = 0.0047, k = 20.0$. D: The system with moderate plasticity: $A = 0.0047, k = 0.7$.

5.2.2 Effect of the Width of the Activation Time Constant (i.e. β)

The parameter β was varied between 0.05 and 0.15 using 40 linearly spaced points (endpoints included). However we will only present results from two parameter values that are representative of mode one and mode two dynamics.

A larger value of β promotes shorter desynchronization durations [11]. For $\beta = 0.124$, the non-plastic system is mode one. The effect of STDP on this system is pre-

sented in Figure 5.4. Across the top and in the upper left corner of Figure 5.4A we see that virtually every point corresponds to a mode one system, as expected. Indeed, a substantial portion of the entire parameter space displays mode one dynamics; about 80% of the parameter space studied.

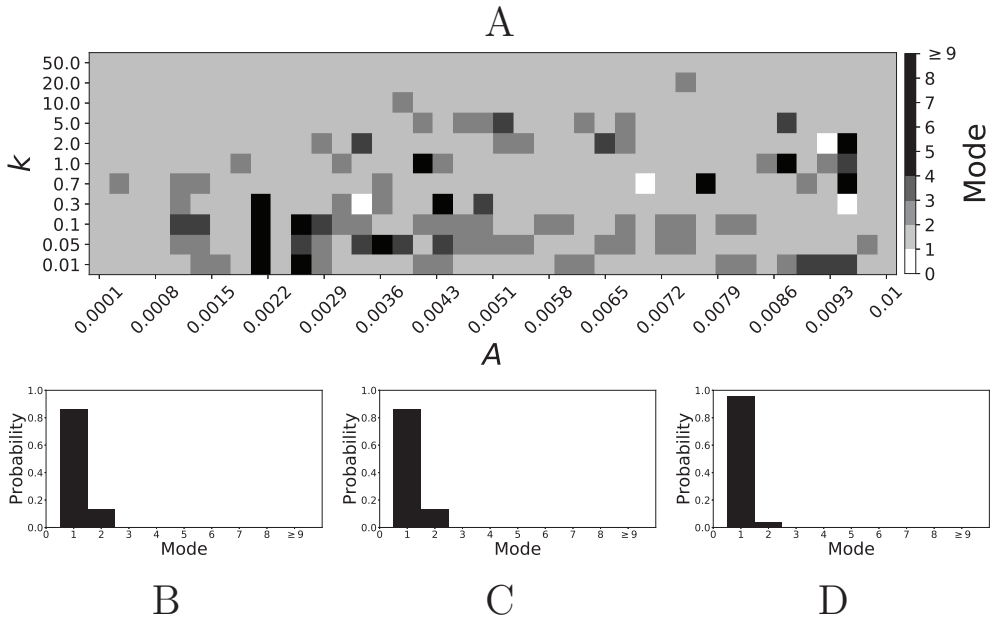

Figure 5.4. A system exhibiting mode one dynamics in the non-plastic case is subjected to plasticity ($\beta = 0.124$). A: Mode is colored via gray scale, see legend on the right of the diagram. The amplitude of the synaptic update, A, is varied along the horizontal axis. The reciprocal of the timescale of the synaptic update, k, is varied along the vertical axis. B, C and D show the changes in the histogram of desynchronization durations as plasticity becomes stronger. B: The system without plasticity. C: The system with very weak plasticity: $A = 0.0052, k = 20.0$. D: The system with moderate plasticity: $A = 0.0052, k = 0.7$.

To illustrate the effect of plasticity on a distribution of desynchronization durations, refer to Figure 5.4B, C and D. Plasticity effects increase from left to right. The introduction of plasticity has a minimal effect on the distribution; there is very little

change visibly. Indeed, the proportion of desynchronization durations of length one increases with plasticity.

Decreasing β increases the mode of a system. If $\beta = 0.091$, the non-plastic system is mode two. With the introduction of very weak plasticity (across the top and the upper left corner of Figure 5.5A) we see that the dynamics are relatively unchanged, i.e. the mode of most systems remains two. However, if plasticity is not very weak, the dynamics shift to mode one in a significant portion of the parameter space. The effect is not as substantial as in the previous section, but about 35% of parameter space becomes mode one (about 45% remains mode 2, i.e. the mode is unchanged).

To illustrate the effect of plasticity on a distribution of desynchronization durations, refer to Figure 5.5B, C and D. Plasticity effects increase from left to right. We see that the vast majority of desynchronization durations become length one as plasticity becomes stronger.

5.2.3 Effect of the Voltage of Half Activation and Maximal Activation for the Activation Time Constant (i.e. v_{w1})

The parameter $vw1$ was varied between 0.06 and 0.18 using 100 linearly spaced points (endpoints included). However we will only presents results from two parameter values that are representative of mode one and mode two dynamics.

Smaller values of v_{w1} result in short desynchronization durations [11]. For $v_{w1} = 0.102$, the non-plastic system is mode one. The effect of STDP on this system is presented in Figure 5.6. We see that mode one dynamics is observed not only for the weak plasticity region (top and upper left corner of Figure 5.6A), but for most of the parameter space (about 85% of the parameter space studied).

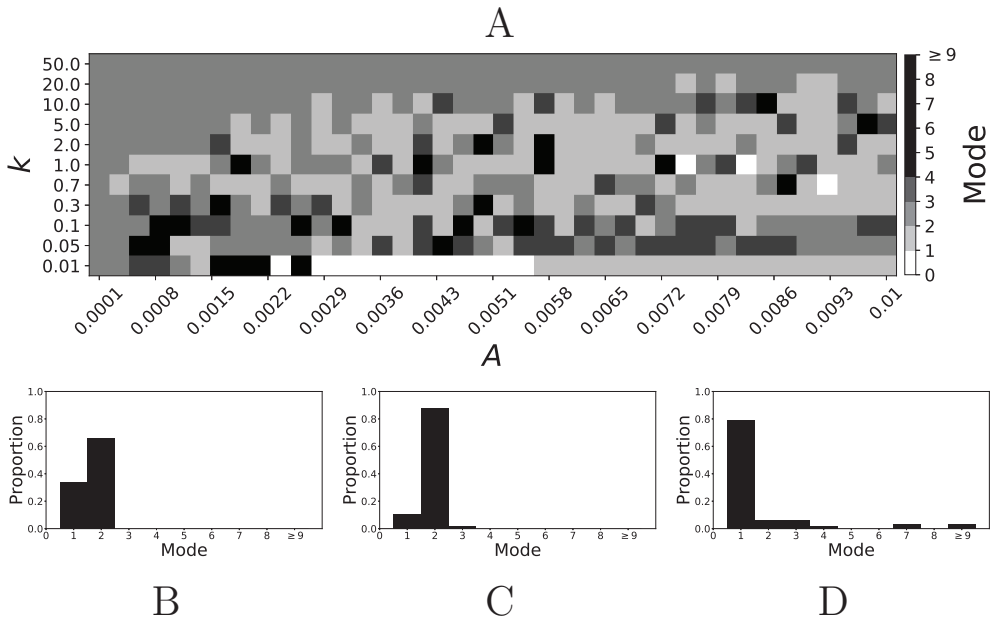

Figure 5.5. A system exhibiting mode two dynamics in the non-plastic case is subjected to plasticity ($\beta = 0.091$). A: Mode is colored via gray scale, see legend on the right of the diagram. The amplitude of the synaptic update, A, is varied along the horizontal axis. The reciprocal of the timescale of the synaptic update, k, is varied along the vertical axis. B, C and D show the changes in the histogram of desynchronization durations as plasticity becomes stronger. B: The system without plasticity. C: The system with very weak plasticity: $A = 0.0047, k = 20.0$. D: The system with moderate plasticity: $A = 0.0047, k = 0.7$.

To illustrate the effect of plasticity on a distribution of desynchronization durations, refer to Figure 5.6B, C and D. Plasticity effects increase from left to right. We see that as plasticity increases to a higher level, the prevalence of mode one is unchanged.

Varying v_{w1} to larger values leads to shorter desynchronization events becoming less prevalent. For $v_{w1} = 0.161$, the non-plastic system is mode two. The effect of STDP is presented in Figure 5.7. When plasticity is added we see that the dynamics

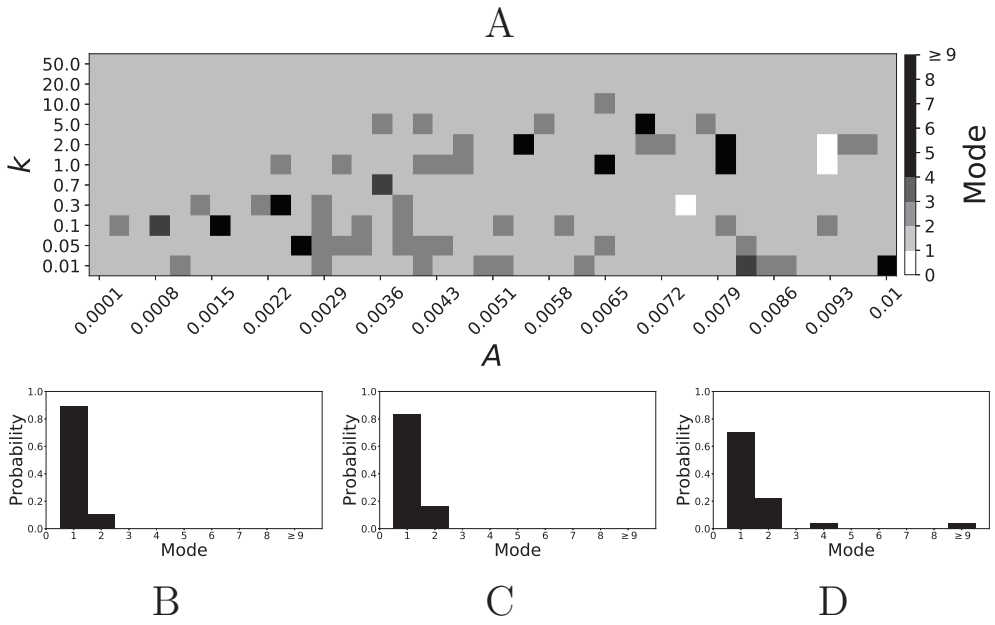

Figure 5.6. A system exhibiting mode one dynamics in the non-plastic case is subjected to plasticity ($v_{w1} = 0.102$). A: Mode is colored via gray scale, see legend on the right of the diagram. The amplitude of the synaptic update, A, is varied along the horizontal axis. The reciprocal of the timescale of the synaptic update, k, is varied along the vertical axis. B, C and D show the changes in the histogram of desynchronization durations as plasticity becomes stronger. B: The system without plasticity. C: The system with very weak plasticity: $A = 0.0047, k = 20.0$. D: The system with moderate plasticity: $A = 0.0047, k = 0.7$.

are similar to the non-plastic case when plasticity is weak enough (top and upper left corner of Figure 5.7A). However, when the plasticity effects are moderate, the system exhibits mode one dynamics frequently (central region of Figure 5.7A). For the domain of parameter space studied, the majority of points (about 45%) correspond to mode one systems, the rest are either mode two (about 40%) or higher.

To illustrate the effect of plasticity on a distribution of desynchronization durations, refer to Figure 5.7B, C and D. Plasticity effects increase from left to right. We

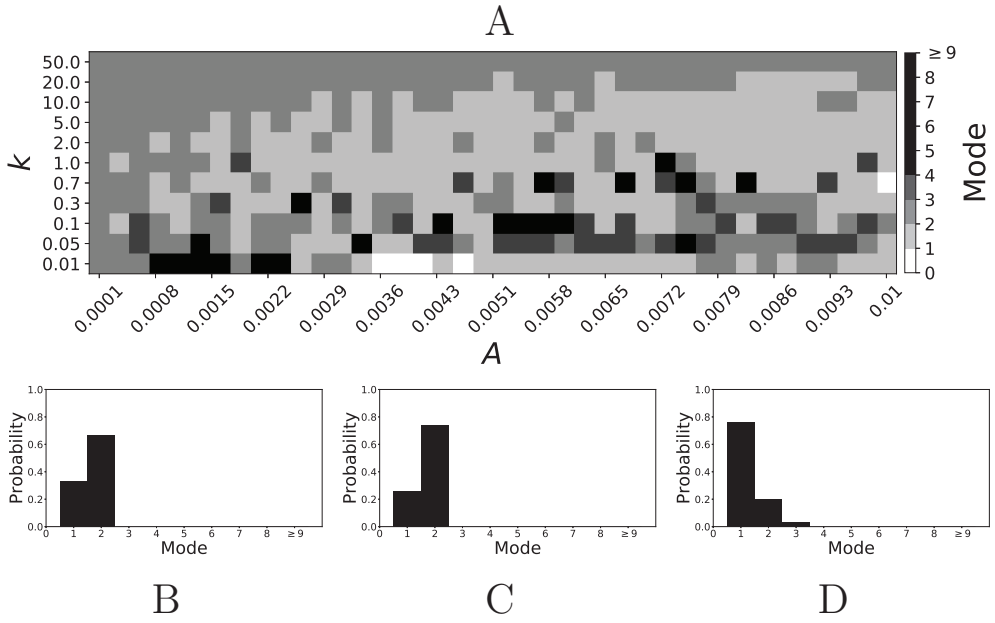

Figure 5.7. A system exhibiting mode two dynamics in the non-plastic case is subjected to plasticity ($v_{w1} = 0.161$). A: Mode is colored via gray scale, see legend on the right of the diagram. The amplitude of the synaptic update, A, is varied along the horizontal axis. The reciprocal of the timescale of the synaptic update, k, is varied along the vertical axis. B, C and D show the changes in the histogram of desynchronization durations as plasticity becomes stronger. B: The system without plasticity. C: The system with very weak plasticity: $A = 0.0047, k = 20.0$. D: The system with moderate plasticity: $A = 0.0054, k = 1.0$.

see that the mode of the system shifts down from two to one as plasticity becomes stronger.

5.2.4 Effect of Simultaneous Changes in β_w and β_τ

The parameter β_w was varied from 0.134 down to 0.94 with 100 linearly spaced points (endpoints included), while β_τ was simultaneously varied from 0.061 up to 0.081 with 100 linearly spaced points. However we will only present results from two

parameter sets that are representative of mode one and mode two dynamics.

Smaller β_w and larger β_τ result in shorter desynchronization durations [11]. For $\beta_w = 0.098, \beta_\tau = 0.079$, the non-plastic system is mode one. Figure 5.8 illustrates the impact of STDP on this system. Mode one dynamics is observed not only for the weak plasticity region (top and upper left corner of Figure 5.8A), but for the majority of the parameter space (about 60% of the parameter space studied).

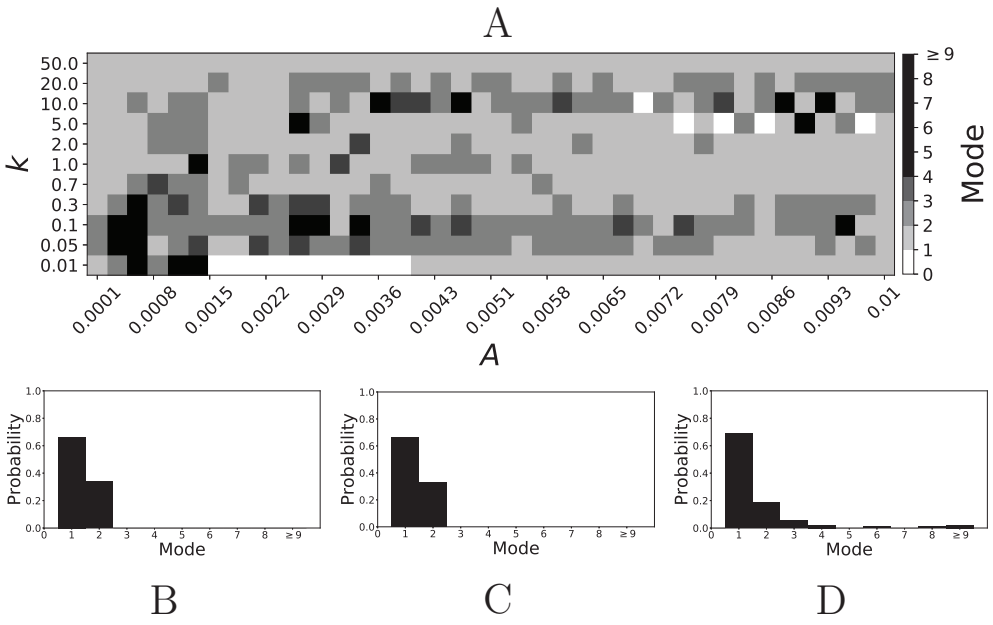

Figure 5.8. A system exhibiting mode one dynamics in the non-plastic case is subjected to plasticity ($\beta_w = 0.098, \beta_\tau = 0.079$). A: Mode is colored via gray scale, see legend on the right of the diagram. The amplitude of the synaptic update, A, is varied along the horizontal axis. The reciprocal of the timescale of the synaptic update, k, is varied along the vertical axis. B, C and D show the changes in the histogram of desynchronization durations as plasticity becomes stronger. B: The system without plasticity. C: The system with very weak plasticity: $A = 0.0049, k = 50.0$. D: The system with moderate plasticity: $A = 0.0052, k = 0.7$.

To illustrate the effect of plasticity on a distribution of desynchronization durations, refer to Figure 5.8B, C and D. Plasticity effects increase from left to right. We see that as plasticity progresses to a moderate level, the proportion of short desynchronizations stays largely unchanged. In particular, the system is still mode one.

If $\beta_w = 0.115, \beta_\tau = 0.071$, the non-plastic system is mode two. Figure 5.9 illustrates the impact of STDP on this system. With the addition of plasticity, we see that the system is largely mode two if the plasticity is weak (top and upper left corner of Figure 5.9A). However, stronger plasticity shifts the dynamics to mode one for a substantial portion of the parameter space (about 55% of points considered).

To illustrate the effect of plasticity on a distribution of desynchronization durations, refer to Figure 5.9B, C and D. Plasticity effects increase from left to right. We see that the distribution is largely unchanged for very weak plasticity, but as plasticity increases, the system becomes mode one.

5.3 Systems with Larger Modes

While results were only presented for systems that were either mode one or mode two in the non-plastic case, the effect of STDP on higher mode systems is generally the same. That is, STDP tends to shift the mode down to one. For example, if $\epsilon = 0.175$ then the non-plastic system is mode three. Figure 5.10 shows the distribution of desynchronization durations when plasticity is added to the system. We fixed the amplitude of the update rule at $A = 0.0024$ and decreased the reciprocal of the timescale k from 50 (5.10(a)) to 20 (5.10(b)) to 10 (5.10(c)). We see that as k decreases (this makes the plasticity effect on the system more prominent) the mode of the system shifts from three to two to one.

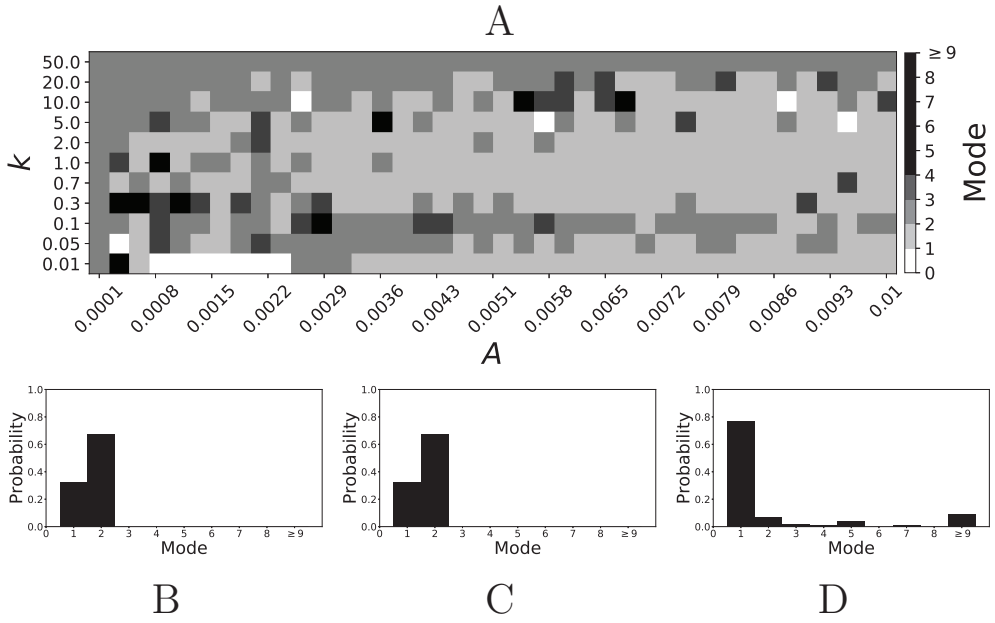

Figure 5.9. A system exhibiting mode two dynamics in the non-plastic case is subjected to plasticity ($\beta_w = 0.115, \beta_\tau = 0.071$). A: Mode is colored via gray scale, see legend on the right of the diagram. The amplitude of the synaptic update, A, is varied along the horizontal axis. The reciprocal of the timescale of the synaptic update, k, is varied along the vertical axis. B, C and D show the changes in the histogram of desynchronization durations as plasticity becomes stronger. B: The system without plasticity. C: The system with very weak plasticity: $A = 0.0049, k = 50.0$. D: The system with moderate plasticity: $A = 0.0054, k = 0.7$.

Finally, we would like to note that there are several points in the parameter space (see Figure 5.2A–Figure 5.9A) that have very large modes. For example, in Figure 5.2 when $A = 0.0006$, $k = 0.01$, the resulting system is mode 38 (i.e. the most common desynchronizations are very long). In these situations the system experiences very long desynchronization events, as opposed to the predominantly short desynchronization durations found in experiments. Generally, these cases have a wide distribution of desynchronization durations, see Figure 5.11. Therefore, while these systems have a large mode, the mode does not present a strong tendency in the

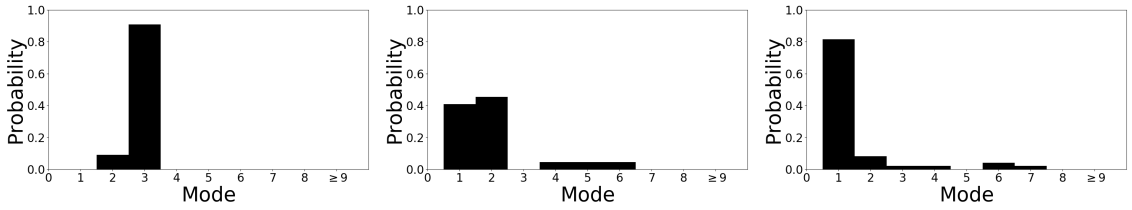

(a) $A = 0.0024$, $k = 50.0$. (b) $A = 0.0024$, $k = 20.0$. (c) $A = 0.0024$, $k = 10.0$.

Figure 5.10. Distribution of desynchronization durations for $\epsilon_1 = 0.175$.

distribution. Nevertheless, these situations are relatively rarely found. For example, when $\epsilon = 0.05$ there are only three out of the 440 simulations that result in a system with a mode of 10 or higher.

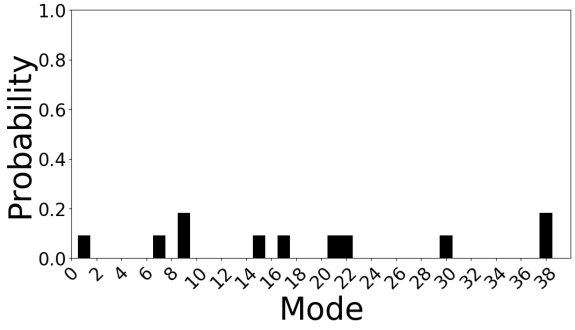

Figure 5.11. Distribution of desynchronization durations for $\epsilon_1 = 0.05$, $A = 0.0006$ and $k = 0.01$. The mode of this system is 38.

5.4 Discussion of Plasticity Impact on Synchrony Patterns

This chapter considered intermittent synchronous dynamics in a small network of simple conductance-based model neurons. While strong synaptic strength can promote synchronization between neurons, moderate values of synaptic coupling lead to dynamics with relatively weak synchronization. It also leads to situations where the episodes of synchronization are interspersed with episodes of desynchronized dynamics. Intermittent synchronization in the presence of moderate (and fixed in time)

coupling is quite typical for coupled oscillatory systems [4]. In other words, temporal variability of correlations is observed due to the relative weakness of a fixed coupling strength. The temporal signatures of this variability have been previously modeled in [11], and were in good agreement with the analysis of the temporal variability observed in experimental data (cf. section 1.4).

However, many actual synapses are plastic and thus the synaptic coupling between neurons experiences temporal variations. This variation may contribute to the temporal variability of intermittent synchrony as well. This chapter considered how one common type of neural plasticity – spike-timing dependent plasticity – might affect this temporal variability. Experimental data ubiquitously points to the prevalence of short desynchronization dynamics in neural synchrony. This kind of dynamics is naturally generated in synaptically coupled conductance-based model neurons. We showed here that the introduction of STDP, under quite general conditions, preserves this realistic fine temporal structure of intermittent neural synchrony. Moreover, when the non-plastic system parameters are selected in such a way as to predominantly express longer desynchronizations, STDP changes the intermittently synchronous dynamics back to one with short desynchronizations. This was observed while varying several different parameters, so that STDP may reverse dynamics from long to short desynchronizations regardless of how the desynchronizations were obtained in the non-plastic system.

The overall dependence of the dynamics on the characteristics of plasticity is quite complicated. Numerical simulations indicate that some plasticity parameter values may promote very unrealistic synchronized dynamics. However, under the conditions considered, the short desynchronization dynamics were obtained in large regions of the parameter space. This was regardless of whether the corresponding non-plastic system was mode one, or had a higher mode.

The results of these numerical simulations suggest that STDP may be one of the contributing factors behind experimentally observed short desynchronization dynamics. Moreover, STDP and cellular mechanisms proposed in [11] may act cooperatively in promoting short desynchronizations.

The results discussed here were obtained in the framework of relatively simple modeling. The actual neuronal synchrony is, of course, a much more complicated phenomenon than the model considered here, and there were multiple factors not included in the model. For example, inhibitory synapses (e.g. [26]). The experimental observations of short desynchronizations were mostly done with LFP and EEG signals, and the network considered here is too simple to adequately model these signals. However, the similarity between experimentally observed intermittent neural synchrony and the temporal patterning of synchrony observed in our study with a relatively simple model with STDP may speak to the very general nature of this phenomenon.

The variability of the dynamics on short time-scales may also be a functionally beneficial phenomenon. Short desynchronization dynamics (which is essentially a high degree of variability of synchrony on very short time-scales) has been conjectured to be conducive for quick and efficient formation and break-up of neural assemblies [11, 14]. As was noted in these studies, the ease of formation and disappearance of synchronized states at rest may suggest that a transient synchronized assembly may be easily formed whenever needed to facilitate a particular function. The results of this chapter suggest that the temporal variability of synaptic strength due to STDP may potentially further facilitate this phenomenon.

6. STOCHASTIC MODEL

In this chapter we implement a neural network consisting of two noisy neurons connected via excitatory synapses, as described in chapter 2. We simulate channel noise, the inherently stochastic nature of the neuronal membrane's ion channels, using first a multiplicative noise term and then an additive term (cf. section 2.4). We will provide evidence that the introduction of noise to the neural network can induce changes in the temporal patterns of synchronization. Specifically, a noise of sufficient strength can shift the distribution of desynchronization durations towards lower values; i.e. noise can promote short desynchronization dynamics over longer desynchronization dynamics. In particular, noise is capable of promoting mode one dynamics. The deterministic variant of this system is discussed in chapter 4. The framework of this chapter is the same as that of chapter 5, except that the mechanism we explore here is noise instead of plasticity.

6.1 Numerical Implementation

Multiplying out the voltage equation from the multiplicative noise section 2.4.1, we obtain the following Langevin-type equation.

$$\frac{\mathrm{d}v_i}{\mathrm{d}t} = A(v) + B(v)\xi_i(t) \tag{6.1}$$

where $A(v)$ and $B(v)$ are the drift and diffusion terms, respectively. In the case of additive noise we simply have

$$\frac{\mathrm{d}v_i}{\mathrm{d}t} = A(v) + \xi_i(t). \tag{6.2}$$

We then solve the system numerically using the Euler-Maruyama method, which is the stochastic analog of the deterministic forward Euler method [20–22]. Here $\xi(t)$

is white noise that is distributed as $\sigma\sqrt{dt}N(0,1)$, where $\sigma \in [0.0, 0.02]$ is the noise strength. This strength interval was chosen such that the noise could be strong enough to effect a change in the network dynamics, yet not completely destroy the inherent spiking dynamics. The noise term for each neuron is generated with a different seed, i.e. the noise terms for the two neurons are uncorrelated.

The initial conditions were $v_{1,0} = 0.1$, $w_{1,0} = 0.376$, $s_{1,0} = 0.86$, $v_{2,0} = -0.29$, $w_{2,0} = 0.127$, $s_{2,0} = 0.64$. These were the same initial conditions as used in the previous study of [11]. The system was solved on the time interval $[0, 20000]$ with a time step of $dt = 0.01$. To account for the initial transient behavior the first 5% of the time-series was discarded. We note that this is sufficient for the system to evolve to some stationary dynamics. We also mention that while an individual solution depends on the initial conditions, the statistical properties that we're interested in (e.g. distribution of desynchronization durations) do not.

Depending on which cellular parameter value was varied, the voltage threshold to define an action potential was set at either 0.20, 0.25 or 0.30. The voltage threshold was initially set at 0.30, however the variation of some parameters induced a decrease in amplitude of the action potentials, which necessitated a change in the voltage threshold. To eliminate the possibility of detecting an action potential immediately after a neuron has fired (caused by the channel noise driving the membrane voltage back over the threshold), a window of 15 ms was set after each neuron's action potential in which we do not count threshold crossings. Since the highest recorded frequency was approximately 40 Hz, a window of 15 ms is appropriate.

6.2 Results of Noise on Synchrony Patterns

In the sections below we present the effects of a multiplicative and an additive noise simultaneously, for each cellular parameter that was varied. The presentation

includes a graph of the mode of the system versus noise strength, synchrony strength versus noise strength, and mean firing frequency versus noise strength. The frequency graph is included as a reminder that certain parameters affect the firing frequency and so the desynchronization durations measured in absolute time units (not cycles of oscillation) may change.

6.2.1 Effect of the Peak Value of the Activation Time Constant (i.e. ϵ)

The parameter ϵ was varied from 0.005 to 0.2 using 100 linearly spaced points (endpoints included). However we will only present results from two parameter values that are representative of mode one and mode two dynamics.

For $\epsilon_1 = 0.044$, the deterministic system is mode one (i.e. the mode of the distribution of all desynchronization event lengths is one cycle of oscillation). Now we include a noise term in the system, one a conductance-based term and the other an additive current term. As the strength of the noise is increased, we see from Figure 6.1 that the system remains mode one. This is true for both the multiplicative and the additive noise case. In addition, the average synchrony index γ and the mean frequency of firing of the system are both approximately constant with respect to the noise strength, see Figures 6.1(b), 6.1(c) and Figures 6.1(e),6.1(f). We also note that these γ and frequency values are very similar to those obtained in [11]. While noise, at a certain intensity, will affect the synchrony strength γ, in our system it appears that noise affects the shape of the waveform first. This could be because our neurons are relaxation oscillations. In any case, this helps explain why γ can be independent of noise, at least for a certain range of noise strengths.

From the previous study of [11] we know that smaller values of ϵ promote shorter desynchronization events. Hence as we increase ϵ to 0.132, the mode of the deterministic system increases to two. From Figure 6.2, we see that as the noise strength is

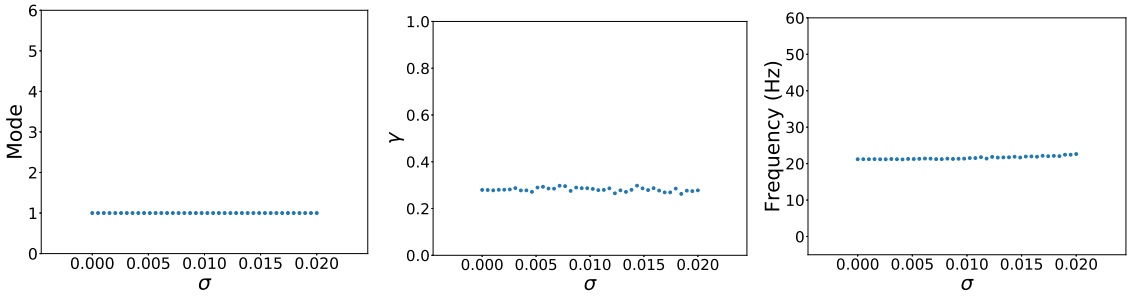

(a) Mode of the system. (b) Synchrony strength γ. (c) Mean firing frequency.

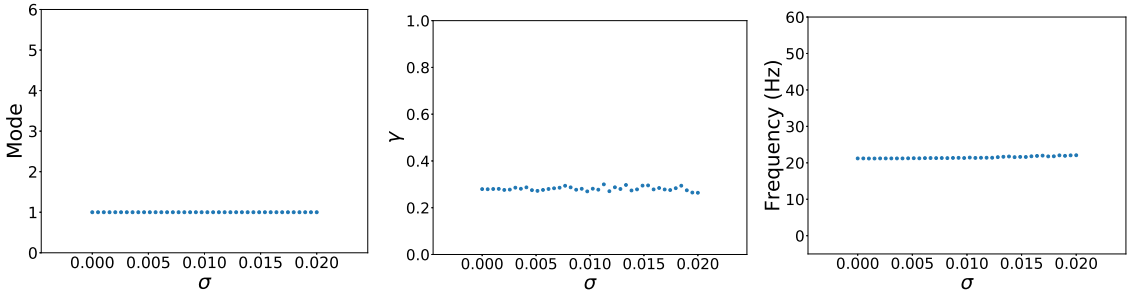

(d) Mode of the system. (e) Synchrony strength γ. (f) Mean firing frequency.

Figure 6.1. A system ($\epsilon_1 = 0.044$) exhibiting mode one dynamics in the deterministic case is subjected to a multiplicative noise in the top row, and an additive noise in the bottom row. The strength of the noise, σ, is varied along the horizontal axes.

increased the mode of the system clearly shifts from two down to one. Once again the average synchrony strength γ and the frequency of firing are nearly constant with respect to the noise strength. Hence the mode of a system can be shifted independently from the synchrony strength γ and the frequency. This indicates that while an input noise may not be sufficiently strong to influence certain properties of the system (such as average synchrony strength or average firing frequency), it may nevertheless influence the dynamics of desynchronization events.

We note that the same trend was observed for systems with larger modes; the addition of a strong enough noise, either conductance-based or an additive current,

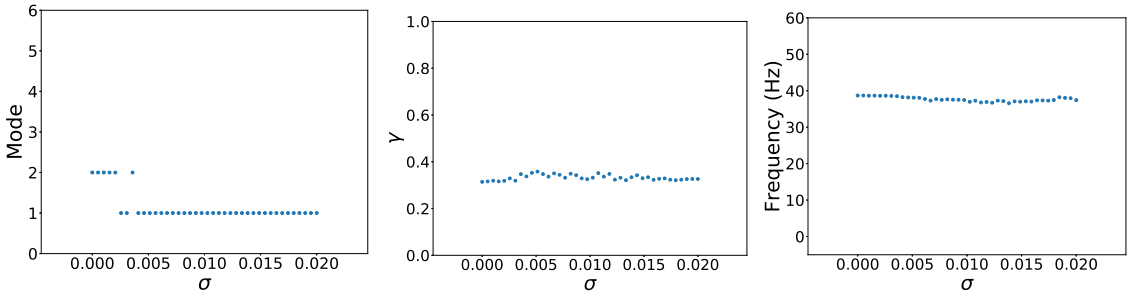

(a) Mode of the system. (b) Synchrony strength γ. (c) Mean firing frequency.

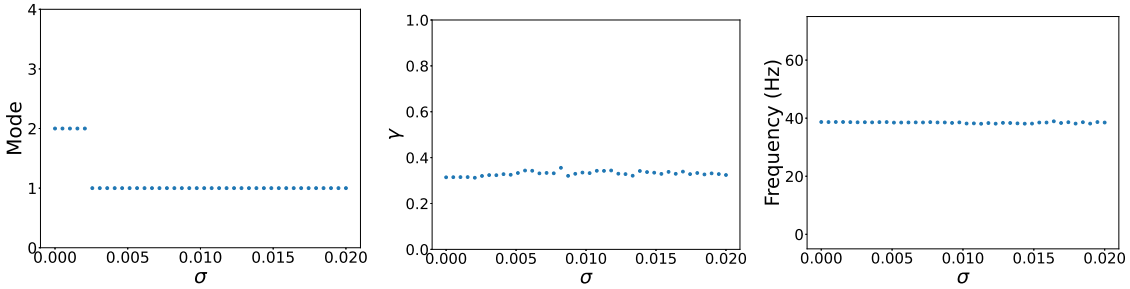

(d) Mode of the system. (e) Synchrony strength γ. (f) Mean firing frequency.

Figure 6.2. A system ($\epsilon_1 = 0.132$) exhibiting mode one dynamics in the deterministic case is subjected to a multiplicative noise in the top row, and an additive noise in the bottom row. The strength of the noise, σ, is varied along the horizontal axes.

served to shift the mode of a system down to one. For example, for $\epsilon_1 = 0.184$ the deterministic system is mode four. However the addition of even a small noise quickly shifted the system to mode one; only 16% of the systems simulated had a mode higher than one. Overall we see that the introduction of a white noise not only preserves mode one dynamics, but at a sufficient strength it can switch mode two (and higher) dynamics down to mode one.

6.2.2 Effect of the Width of the Activation Time Constant (i.e. β)

The parameter β was varied between 0.05 and 0.15 using 100 linearly spaced points (endpoints included). However we will only present results from two parameter values

that are representative of mode one and mode two dynamics.

For $\beta = 0.131$, the deterministic system is mode one. We see in Figure 6.3 that the mode of the system is unchanged as noise is added and its strength is increased. This is true for both the multiplicative and additive noise case. The synchrony strength γ and the frequency of the system are likewise virtually unchanged from that of the deterministic system, see Figures 6.3(b),6.3(c) and Figures 6.3(e),6.3(f).

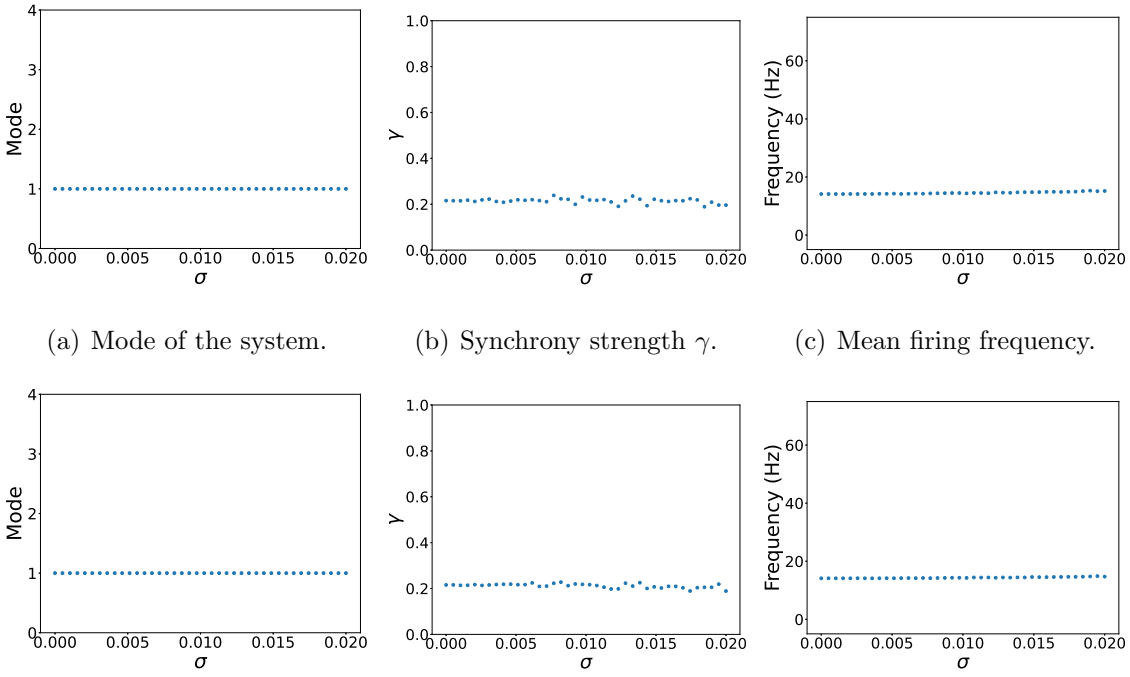

(a) Mode of the system. (b) Synchrony strength γ. (c) Mean firing frequency.

(d) Mode of the system. (e) Synchrony strength γ. (f) Mean firing frequency.

Figure 6.3. A system ($\beta = 0.131$) exhibiting mode one dynamics in the deterministic case is subjected to a multiplicative noise in the top row, and an additive noise in the bottom row. The strength of the noise, σ, is varied along the horizontal axes.

From the previous study of [11] we know that a larger value of β promotes shorter desynchronization durations. When we set $\beta = 0.080$, the deterministic system is mode two. We see in Figure 6.4 that for small noise strengths the system remains

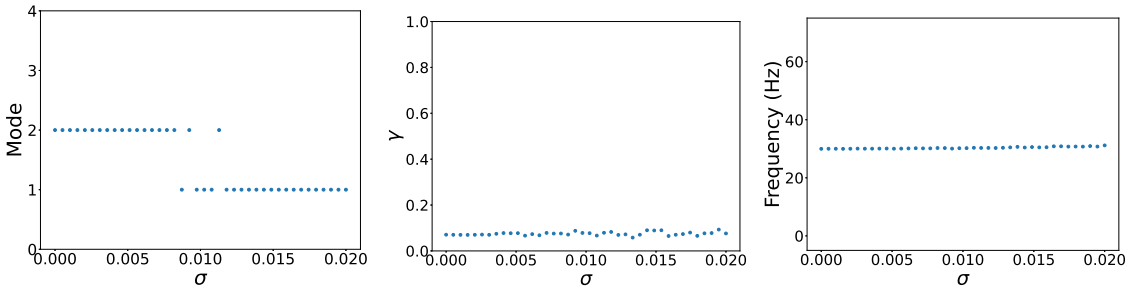

(a) Mode of the system. (b) Synchrony strength γ. (c) Mean firing frequency.

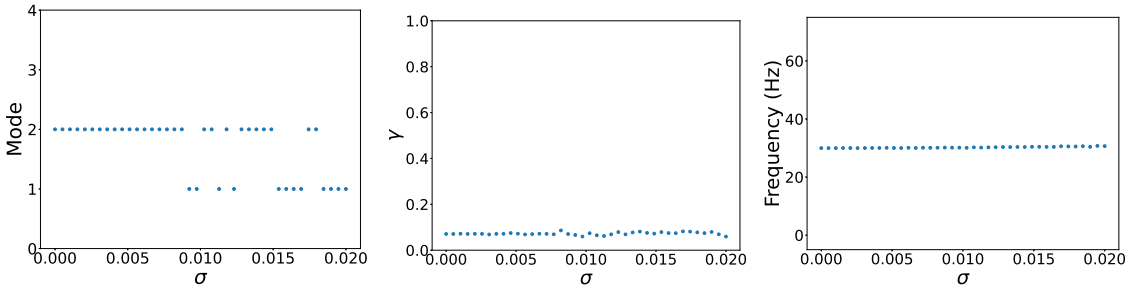

(d) Mode of the system. (e) Synchrony strength γ. (f) Mean firing frequency.

Figure 6.4. A system ($\beta = 0.080$) exhibiting mode two dynamics in the deterministic case is subjected to a multiplicative noise in the top row, and an additive noise in the bottom row. The strength of the noise, σ, is varied along the horizontal axes.

mode two, but once the strength reaches a sufficiently large value the system becomes mode one. Again, the shift in mode is independent of the average synchrony index or the mean firing frequency, see Figures 6.4(c),6.4(b) and Figures 6.4(f),6.4(e).

6.2.3 Effect of the Voltage of Half Activation and Maximal Activation for the Activation Time Constant (i.e. v_{w1})

The parameter v_{w1} was varied between 0.06 and 0.18 using 100 linearly spaced points (endpoints included). However we will only presents results from two parameter values that are representative of mode one and mode two dynamics.

For $v_{w1} = 0.096$, the deterministic system is mode one. The effect of introducing a noise term to the system is shown in Figure 6.5. In Figures 6.5(a) and 6.5(d) we see that the mode one dynamics is preserved for all noise strengths, regardless of whether the noise is multiplicative or additive.

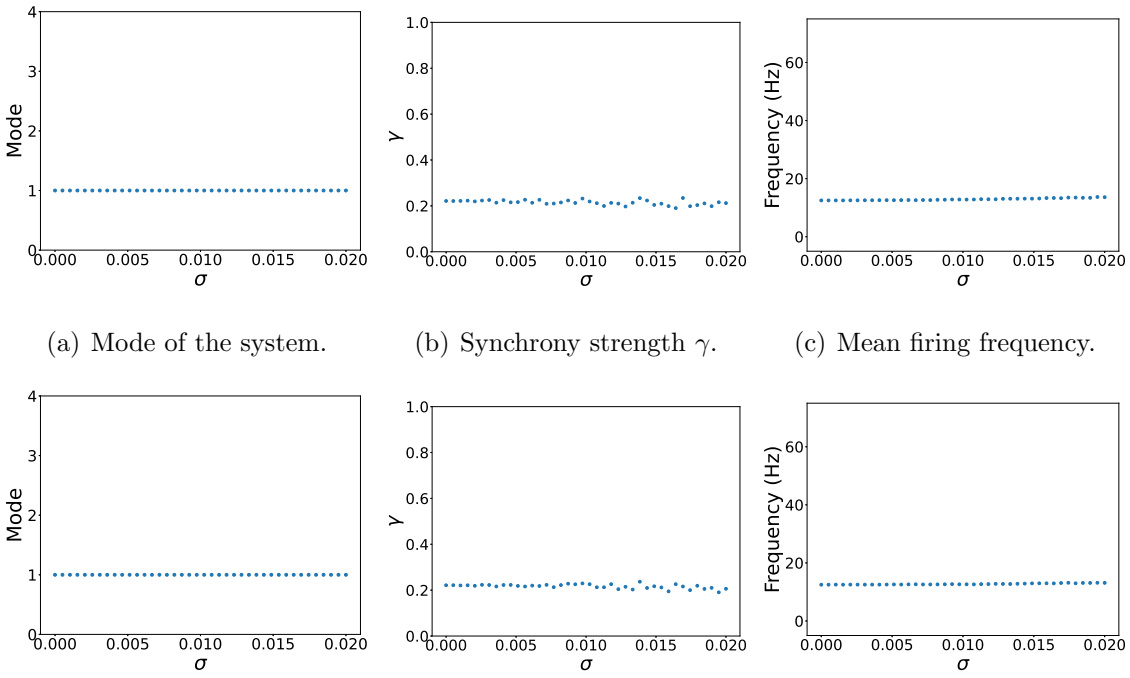

(a) Mode of the system. (b) Synchrony strength γ. (c) Mean firing frequency.

(d) Mode of the system. (e) Synchrony strength γ. (f) Mean firing frequency.

Figure 6.5. A system ($v_{w1} = 0.096$) exhibiting mode one dynamics in the deterministic case is subjected to a multiplicative noise in the top row, and an additive noise in the bottom row. The strength of the noise, σ, is varied along the horizontal axes.

Smaller values of v_{w1} result in shorter desynchronization durations [11]. Hence if we let $v_{w1} = 0.169$, the deterministic system becomes mode two. In the stochastic system, a strong enough noise will shift the mode to one, this is illustrated in Figure 6.6. While the shift in the graph is perhaps not as clean as in previous figures, it is still a definitive shift. Definitive meaning that a stronger noise tends to push the

system towards mode one dynamics, and rarely increases the mode.

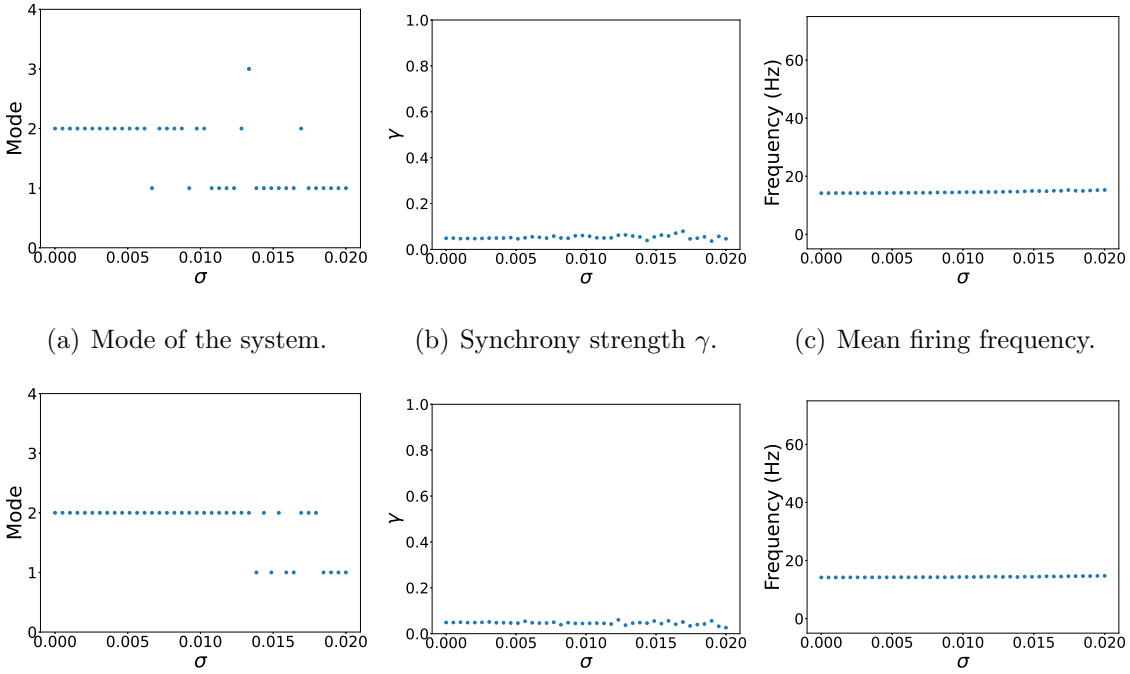

(a) Mode of the system. (b) Synchrony strength γ. (c) Mean firing frequency.

(d) Mode of the system. (e) Synchrony strength γ. (f) Mean firing frequency.

Figure 6.6. A system ($v_{w1} = 0.169$) exhibiting mode two dynamics in the deterministic case is subjected to a multiplicative noise in the top row, and an additive noise in the bottom row. The strength of the noise, σ, is varied along the horizontal axes.

6.2.4 Effect of Simultaneous Changes in β_w and β_τ

The parameter β_w was varied from 0.134 down to 0.94 with 100 linearly spaced points (endpoints included), while β_τ was simultaneously varied from 0.061 up to 0.081 with 100 linearly spaced points. However we will only present results from two parameter sets that are representative of mode one and mode two dynamics.

Variation of the previous parameters, i.e. ϵ, β and v_{w1}, can affect the average synchronization strength and frequency of firing in addition to changing the durations

of desynchronizations. For example, a typical stochastic system with a parameter of $\beta = 0.065$ has a frequency of about 41 Hz and was either mode one, two or three depending on the noise strength. While a typical stochastic system with a parameter of $\beta = 0.131$ has a frequency of about 14 Hz and was constantly mode one, irregardless of the noise strength used. To control the mode of a deterministic system while keeping both the average synchrony strength and firing frequency near constant, one can take the parameter β and separate it into two independent parameters, β_τ and β_w. The result is that the mode of the system is nearly independent of the synchrony strength and frequency and value of the cellullar parameters β_w, β_τ [11]. From the same study we know that smaller β_w and larger β_τ will result in shorter desynchronization durations.

For $\beta_w = 0.098$ and $\beta_\tau = 0.079$ the deterministic system is mode one. As illustrated in Figure 6.7, the mode remains one as the strength of the noise in the stochastic system is increased.

For $\beta_w = 0.120$ and $\beta_\tau = 0.068$ the deterministic system is mode two. In the stochastic version of this system the mode is switched from two to one with a sufficiently large noise strength, see Figure 6.8. We point out that the frequencies and synchrony strengths seen in Figure 6.7 and Figure 6.8 are nearly identical, as was the goal in creating the β_w, β_τ parameters.

6.3 Discussion of Noise Impact on Synchrony Patterns

Here we have simulated a small network of weakly coupled conductance-based neurons, and what was observed was a weak synchronization that varied in time. That is to say, the network experienced periods of synchrony that were interspersed with periods of desynchronized activity. This is consistent with the previous study of [11] where the network was the same as here, only deterministic. It is also consis-

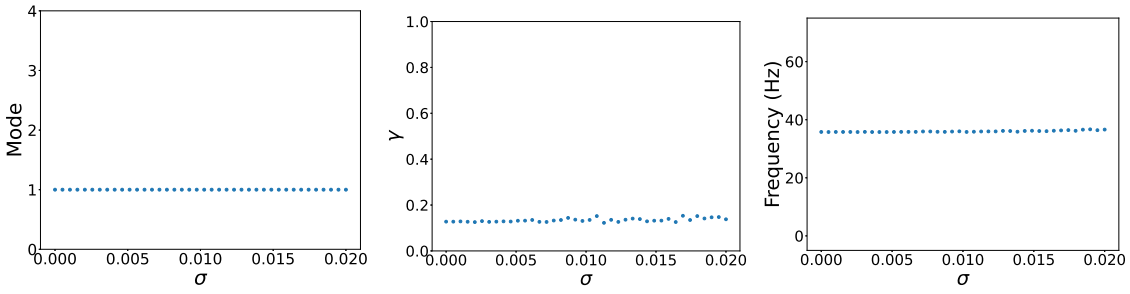

(a) Mode of the system. (b) Synchrony strength γ. (c) Mean firing frequency.

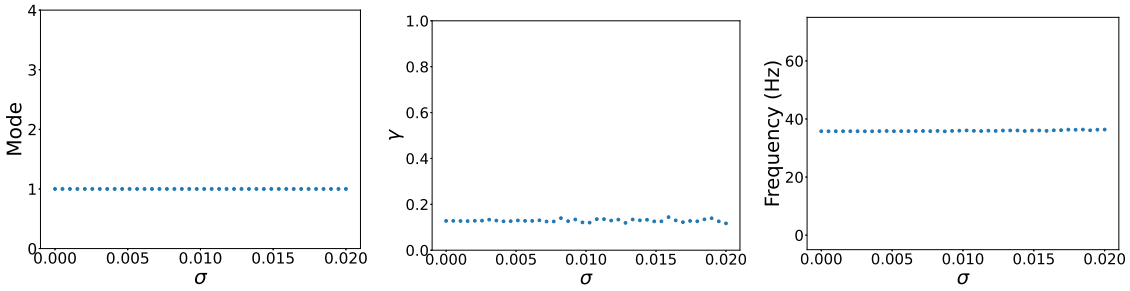

(d) Mode of the system. (e) Synchrony strength γ. (f) Mean firing frequency.

Figure 6.7. A system ($\beta_w = 0.098$, $\beta_\tau = 0.079$) exhibiting mode one dynamics in the deterministic case is subjected to a multiplicative noise in the top row, and an additive noise in the bottom row. The strength of the noise, σ, is varied along the horizontal axes.

tent with the findings from previous studies using experimental data (see section 1.4).

Naturally, real biological neurons are noisy oscsillators, and there may be many sources of this noise [9, 19, 23]. To understand whether this stochasticity affects the temporal variations in the intermittent synchrony of the network, we considered two methods of adding noise resulting from the opening and closing of ion channels. The first, was directly adding a zero mean Gaussian process to the activation variable for potassium current. The second was to add a zero mean Gaussian process directly to the voltage equation. One main difference between the methods is that the first is a multiplicative noise and the second is additive. While there may not be a general

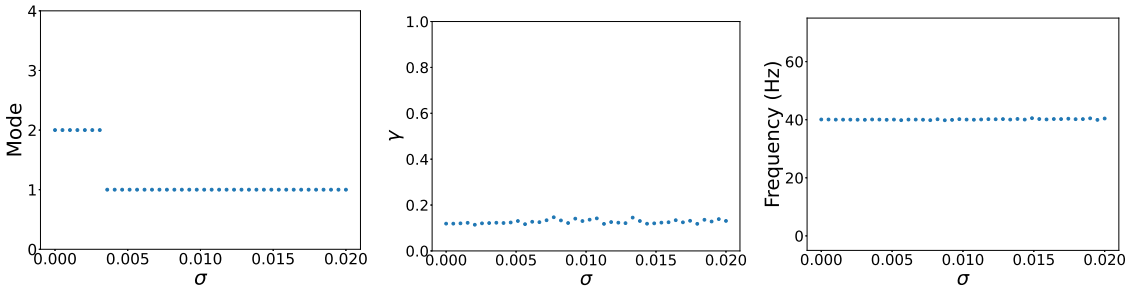

(a) Mode of the system. (b) Synchrony strength γ. (c) Mean firing frequency.

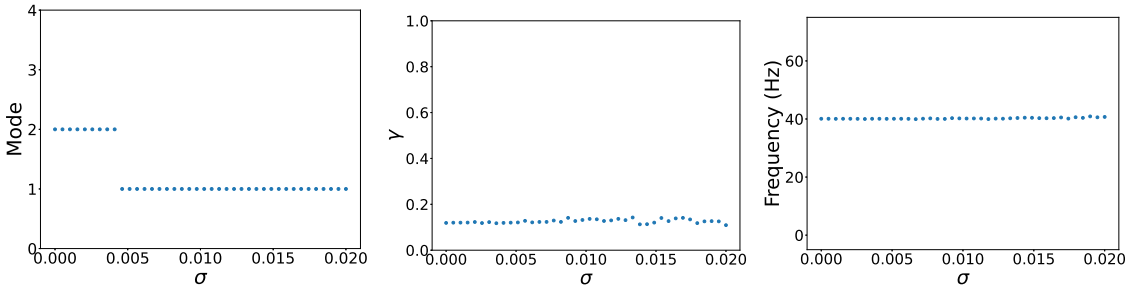

(d) Mode of the system. (e) Synchrony strength γ. (f) Mean firing frequency.

Figure 6.8. A system ($\beta_w = 0.120$, $\beta_\tau = 0.068$) exhibiting mode two dynamics in the deterministic case is subjected to a multiplicative noise in the top row, and an additive noise in the bottom row. The strength of the noise, σ, is varied along the horizontal axes.

consensus, we note that [10] recommend using a multiplicative noise as it can be mathematically related back to Markov chain models. Regardless, we used both and found that their introduction preserved the temporal variability in the intermittent synchrony that was found in previous studies. In addition, if the deterministic system had a mode higher than one (i.e. the desynchronization durations tended to be longer) then the introduction of noise (at a sufficient strength) could shift the network down to mode one dynamics. This was found across all cellular parameters that were varied.

Another potentially significant source of noise is that from the synapses. However, since we consider very weak coupling between the neurons (g_{syn} is orders of magnitude

less than g_K) no addition of noise to the synaptic variable (which is bounded between zero and one) could induce a significant change in the system. This was verified numerically across a wide range of synaptic noise strengths.

7. CONCLUSION

This thesis studied the synchronous dynamics in a neural network consisting of two simple conductance-based model neurons. The dynamics are inherently intermittent, or variable in time, due to the weak synaptic coupling. This means that the network exhibits episodes of synchronization that are separated by episodes of desynchronization. This is not a unique phenomenon, indeed it is quite common in coupled oscillatory systems [4]. What is interesting is that a particular type of intermittent synchronous dynamics is prevalent in real neural systems across multiple species and brain areas (cf. section 1.4). This particular type is a regime where the neural system leaves its synchronized state frequently, but only remains desynchronized for a short period of time. We again mention that we measure "time" in terms of cycles of oscillations. The previous work of [11] modeled this phenomenon in a simple and general setting. The results presented in this thesis extend this previous work by adding complexities to the model in the form of synaptic plasticity and channel noise.

Incorporating spike-timing dependent plasticity (a very common variety of synaptic plasticity) to the model allows the synaptic conductances (a measure of the strength of the coupling) to vary with time. Since many actual synapses are plastic, it is possible that the temporal variations in the synaptic conductances influence the temporal variations in the patterns of synchrony. The numerical results presented in chapter 5 indicate that the addition of STDP *does* affect the synchronization dynamics in our model network. It was observed that STDP preserved mode one dynamics if the non-plastic system was mode one, and that STDP tended to depress the mode of the system towards one if the non-plastic system had a mode greater than one. These results were consistent across large regions of the two-dimensional plasticity parameter space. These results were also observed while varying several different

cellular parameters. Hence it seems a general phenomenon that plasticity promotes predominantly short desynchronization dynamics over longer desynchronizations, at least under certain conditions.

The exact relationship between the synchronization dynamics and the properties of plasticity is probably quite complicated and, at this moment, unknown. For example, there were isolated points in the parameter space where the numerical analysis showed unrealistically large mode values. It is not known why this occurs, perhaps it is a result of our particular definition of synchrony and the partitioning of the phase space into quadrants (as versus a different partition). However it was generally observed that for these large mode cases, the distribution of desynchronization durations is usually quite broad; hence the mode of the distribution is not necessarily very descriptive.

Next, we return to the non-plastic model and add a stochastic term meant to model ion channel noise that is inherent in real biological neurons. This was done in two separate ways: a conductance-based noise and a current noise. Noise has been shown to have the ability to either enhance or degrade properties, including synchronization, of neural systems [23]. Again, since actual neurons are inherently noisy, it is possible that noise could affect the synchronization dynamics. The numerical results presented in chapter 6 show that both types of channel noise preserve the mode one dynamics that was observed in their deterministic counterpart systems. In addition, if the deterministic system favored longer desynchronization durations over shorter ones (i.e. the mode of the system was greater than one), then a sufficiently strong noise could induce a shift towards mode one dynamics. These results were observed consistently across the variation of several different cellular parameters.

There are various sources of noise in neural systems, a significant one being channel noise. Another significant source is that from the synaptic channels. However,

since we consider very weak coupling between the neurons (g_{syn} is orders of magnitude less than g_K) no addition of noise to the synaptic variable (which is bounded between zero and one) could induce a significant change in the system.

The models used throughout this thesis are simple and therefore have their limitations. For instance, the effect of inhibitory synapses was not studied. The scale of the model is quite small which limits the complexity of dynamics that it is able to produce. The synchronization dynamics within a stochastic and simultaneously plastic neural system was not studied. Only one type of plasticity was implemented. Only two ionic species were included in the model. Yet despite these limitations, these models were able to recreate the short desynchronization dynamics that is observed in real neural systems.

Synaptic plasticity, noise and synchronization are all ubiquitous throughout neural systems. Here we have used mathematical modeling to study the impact of synaptic plasticity, and separately, noise on the temporal patterning of synchronization within these neural systems. We provide numerical evidence that synaptic plasticity and channel noise may be potential mechanisms behind the observed short desynchronization dynamics. This, along with previous experimental evidence, indicates that this specific temporal patterning of synchronization is a very general and robust phenomenon within neural systems.

REFERENCES

[1] Izhikevich, E. M. *Dynamical Systems in Neuroscience: The Geometry of Excitability and Bursting.* Cambridge, MA: MIT Press, 2007.

[2] Ermentrout, G. B. and Terman, D. H. *Mathematical Foundations of Neuroscience.* New York, NY: Springer, 2010.

[3] Dayan, Peter and Abbott L.F. *Theoretical Neuroscience: Computational and Mathematical Modeling of Neural Systems.* Cambridge, MA: MIT Press, 2001.

[4] Pikovsky, A., Rosenblum, M., and Kurths, J. *Synchronization: A Universal Concept in Nonlinear Sciences.* Cambridge: Cambridge University Press, 2001.

[5] Morris C, Lecar H. *Voltage oscillations in the barnacle giant muscle fiber.* Biophys J 35:193–213, 1981.

[6] Feldman, D. *The spike timing dependence of plasticity.* Neuron. 75(4): 556–571, 2012.

[7] Zhang, L., Tao H. W., Holt C. E., Harris W. A., Poo M. *A critical window for cooperation and competition among developing retinotectal synapses.* Nature. 395(6697): 37–44, 1998.

[8] Zhigulin, V. P., Rabinovich, M. I., Huerta, R., and Abarbanel, H. D. *Robustness and enhancement of neural synchronization by activity-dependent coupling.* Phys Rev E Stat Nonlin Soft Matter Phys. 67: 021901, 2003.

[9] Faisal, A. A., Selen, L. P. J., and Wolpert, D. M. *Noise in the nervous system.* Nat Rev Neurosci. 9(4): 292–303, 2008.

[10] Goldwyn JH, Shea-Brown E. *The What and Where of Adding Channel Noise to the Hodgkin-Huxley Equations.* PLoS Comput Biol 7(11): e1002247, 2011. https://doi.org/10.1371/journal.pcbi.1002247

[11] Ahn S., Rubchinsky LL. *Potential Mechanisms and Functions of Intermittent Neural Synchronization.* Front. Comput. Neurosci. 11:44, 2017.

[12] Ahn S., Park C., Rubchinsky LL. *Detecting the temporal structure of intermittent phase locking.* Phys. Rev. E Stat. Nonlin. Soft Matter Phys. 84: 016201, 2011.

[13] Rubchinsky, L., Park, C. and Worth, R.M. *Intermittent neural synchronization in Parkinson's disease.* Nonlinear Dyn 68, 329–346, 2012. https://doi.org/10.1007/s11071-011-0223-z

[14] Ahn S., Rubchinsky LL. *Short desynchronization episodes prevail in synchronous dynamics of human brain rhythms.* Chaos 23: 013138, 2013.

[15] Abbott L., and Nelson, S. *Synaptic plasticity: taming the beast.* Nature neuroscience. 3 Suppl. 1178-83. 10.1038/81453.

[16] Feldman, D. *The Spike-Timing Dependence of Plasticity.* Neuron. 75. 556-71. 10.1016/j.neuron.2012.08.001.

[17] Nowotny, T., Zhigulin, V.P., Selverston, A.I., Abarbanel, H.D., Rabinovich, M.I. *Enhancement of synchronization in a hybrid neural circuit by spike-tming dependent plasticity.* J. Neurosci. 23:9776-9785.

[18] Knoblauch, A., Hauser, F., Gewaltig, M.O., Körner, E., Palm, G. *Does spike-timing dependent synaptic plasticity couple or decouple neurons firing in synchrony?* Front. Comput. Neurosci. 6:55.

[19] Laing, Carlo, and Gabriel J. Lord. *Stochastic Methods in Neuroscience.* Oxford: Oxford University Press, 2010.

[20] Kloeden, P.E., and Platen, E. *Numerical Solution of Stochastic Differential Equations.* Berlin; New York: Springer-Verlag, 1992.

[21] Gardiner, C. *Stochastic Methods.* Berlin; Heidelberg: Springer-Verlag, 2009.

[22] Higham, D.J. *An Algorithmic Introduction to Numerical Simulation of Stochastic Differential Equations.* SIAM Review. Vol. 43, No. 3: 525–546, 2001.

[23] Ermentrout, G. B., Galán, R. F., Urban, N.N. *Relability, synchrony and noise.* Trends Neurosci. 31(8): 428–434, 2008.

[24] Buck, J. and Buck, E. *Synchronous Fireflies.* Scientific American. Vol. 234, No. 5: 74-85, 1976.

[25] Strogatz, S.H. and Stewart, I. *Coupled Oscillators and Biological Synchronization.* Scientific American. 269(6): 102-109, 1993.

[26] Nowotny, T., Huerta, R., and Rabinovich, M. I. *Neural synchrony: peculiarity and generality.* Chaos 18: 037119, 2008.

[27] Erra, G.R., Velazquez, P., and Rosenblum, M. *Neural Synchronization from the Perspective of Non-linear Dynamics.* Front. Comput. Neurosci. 11:98, 2017.

[28] Uhlhaas, P.J., Pipa G, Lima B, et al. *Neural synchrony in cortical networks: history, concept and current status.* Front Integr Neurosci. 3:17, 2009.

[29] Buzasaki, G. *Rhythms of the Brain.* Oxford: Oxford University Press.

[30] Usrey, W.M., and Reid, R.C. *Synchrony Activity in the Visual System.* Annu. Rev. Physiol. 61:435-56, 1999.

[31] Marder, E., and Calabrese, R.L. *Principles of Rhythmic Motor Pattern Generation.* Physiological Reviews. Vol. 76, No. 3, 1996.

[32] Brette, R. *Computing with Neural Synchrony.* PLoS Comput. Biol. 8(6): e1002561.

[33] Fell, J., Axmacher, N. *The role of phase synchronization in memory processes.* Nat Rev Neurosci. 12(2):105-118, 2011.

[34] Uhlhaas, P.J., and Singer, W. *Neural Synchrony in Brain Disorders: Relevance for Cognitive Dysfunctions and Pathophysiology.* Neuron. 52: 155-168, 2006.

[35] Spencer, K.M., Nestor, P.G., Niznikiewicz, M.A., Salisbury, D.F., Shenton, M.E, McCarley, R.W. *Abnormal Neural Synchrony in Schizophrenia.* J. Neurosci. 23(19): 7407-7411, 2003.

[36] Schwab B.C., Heida T., Zhao Y., Marani E., van Gils S.A., van Wezel R.J. *Synchrony in Parkinson's disease: importance of intrinsic properties of the external globus pallidus.* Front Syst Neurosci. 7:60, 2013.

[37] Popovych O.V., Tass P.A. *Control of abnormal synchronization in neurological disorders.* Front Neurol. 5:268, 2014.

[38] Uhlhaas, P., Singer, W. *Abnormal neural oscillations and synchrony in schizophrenia.* Nat. Rev. Neurosci. 11: 100–113, 2010.

[39] Rabinovich, M., Huerta, R., and Laurent, G. *Transient dynamics for neural processing.* Science 321: 48–50, 2008.

[40] Park, C., Worth, R. M., and Rubchinsky, L. L. *Fine temporal structure of beta oscillations synchronization in subthalamic nucleus in Parkinson's disease.* J. Neurophysiol.103: 2707–2716, 2010.

[41] Ratnadurai-Giridharan, S., Zauber, S. E., Worth, R. M., Witt, T., Ahn, S., and Rubchinsky, L. L. *Temporal patterning of neural synchrony in the basal ganglia in Parkinson's disease.* Clin. Neurophysiol. 127: 1743–1745, 2016.

[42] Ahn, S., Zauber, S. E., Witt, T., Worth, R. M., and Rubchinsky, L. L. *Neural synchronization: Average strength vs. temporal patterning.* Clin. Neurophysiol. 129: 842-844, 2018.

[43] Ahn, S., Rubchinsky, L. L., and Lapish, C. C. *Dynamical reorganization of synchronous activity patterns in prefrontal cortex - hippocampus networks during behavioral sensitization.* Cereb. Cortex 24: 2553–2561, 2014.

[44] Malaia, E., Ahn, S., and Rubchinsky, L. L. *Dysregulation of temporal dynamics of synchronous neural activity in adolescents on autism spectrum.* Autism Res. 13:24, 2020.

[45] Guckenheimer, J., and Holmes, P. *Nonlinear Oscillations, Dynamical Systems, and Bifurcations of Vector Fields.* New York: Springer-Verlag, 1986.

[46] Hirsch, M.W., Smale, S., Devaney, R.L. *Differential Equations, Dynamical Systems, and an Introduction to Chaos.* San Diego, CA: Academic Press, 2004.

[47] Zirkle J., Rubchinsky, LL. *Spike-Timing Dependent Plasticity Effect on the Temporal Patterning of Neural Synchronization.* Front. Comput. Neurosc., 2020.

VITA

EDUCATION

- **Ph.D. Candidate in Applied Mathematics, Indiana University - Purdue University Indianapolis (IUPUI). 2015–2020.**
  Advisor: Dr. Leonid Rubchinsky. My area is dynamical systems as they apply to neuroscience. My research involves mathematical modeling, numerical simulations, analysis of time-series and data visualization.
- **MS in Applied Statistics, IUPUI. 2017–2019.**
- **BS with Highest Distinction in Pure Mathematics, IUPUI. 2011-2015.**
- **BS in Physics, IUPUI. 2011–2015.**
- **Minor in Chemistry, IUPUI. 2011–2014.**

WORK AND TEACHING EXPERIENCE

- **Graduate Student Instructor, Dept. of Mathematics, IUPUI. 2015–2020.**
  - Business Calculus (M119) Spring 2016, Summer 2016.
  - Trigonometry (MA15400) Fall 2016, Spring 2017, Fall 2017, Summer 2018.
  - Fundamentals of Algebra I (MA11000) Fall 2017.
  - Calculus I (MA16500) Spring 2018, Fall 2018.
  - College Algebra (MA15300) Spring 2019.
  - Multidimensional Math (MA17100) Summer 2019.
  - Calculus I for Life Sciences (MA23100) Fall 2019.
  - Calculus II for Life Sciences (MA23200) Spring 2020, Summer 2020.

- **Assistant Manager, Mathematics Assistance Center (MAC) @ IUPUI. 2014–2015.**

  Oversaw daily operations for a facility that employed 100+ persons. Directly managed a team of approximately 10-15 students who tutored calculus. I spearheaded the conversion of Word documents to LaTeX, including the production of a 150+ page reference for the first-semester of calculus. I also produced an in-depth 35+ page reference guide for LaTeX.

- **Calculus Tutor, MAC @ IUPUI. 2013–2014.**

  Tutored mathematics ranging from basic algebra to differential equations.

- **Physics Tutor, Physics Learning Space @ IUPUI. Fall 2012.**

  Tutored students taking first-year physics courses.

PUBLICATIONS

- J Zirkle, LL Rubchinsky (2019) Exploring mechanisms of intermittent patterns of neural synchrony. *BMC Neuroscience*, 20(Suppl 1): P270.
- Zirkle J., Rubchinsky, LL (2020) Spike-Timing Dependent Plasticity Effect on the Temporal Patterning of Neural Synchronization. *Front. Comput. Neurosc.*

PRESENTATIONS

- Graduate Student Seminar, Fall 2015. *Bernoulli Polynomials and Numbers.*
- Graduate Student Seminar, Fall 2016. *State of Stress and Strain.*
- Graduate Student Seminar, Spring 2017. *Pattern Formation Mechanisms.*
- On-campus SIAM event, Fall 2017. *Synchronization between Weakly Coupled Neurons.*
- Graduate Student Seminar, Fall 2017. *Molecular Dynamics.*
- 2018 Annual Meeting for Greater Indiana Society for Neuroscience. *Spike-timing-dependent plasticity effect on the patterns of neural synchrony.*

- Computational and Systems Neuroscience Symposium. IUPUI 2018. *Spike-timing-dependent plasticity effect on the patterns of neural synchrony.*
- Graduate Student Seminar, Spring 2019. *Introduction to Stochastic Differential Equations.*
- Graduate Student Seminar, Fall 2019. *Single Neuron Dynamics.*
- Graduate Student Seminar, Spring 2020. *Structural Stability of nonlinear ODE systems.*

AWARDS

- Graduate Student Teaching Award, Spring 2018.
- 2015 Yuri Abramovich Memorial Scholarship.
- 2015 Pure Math Outstanding Senior.